Tuning stiffness of hyaluronan-cholesterol nanogels by mussel-inspired dopamine-Fe^{3+} coordination: Preparation and properties evaluation

Ju Wang [a], Benedetta Brugnoli [b], Federica Foglietta [c], Ilaria Andreana [c], Giovanni Longo [d], Simone Dinarelli [d], Marco Girasole [d], Loredana Serpe [c], Silvia Arpicco [c], Iolanda Francolini [b], Chiara Di Meo [a], Pietro Matricardi [a,*]

[a] *Departments of Drug Chemistry and Technologies, Sapienza University of Rome, Piazzale Aldo Moro 5, Rome, 00185, Italy*
[b] *Department of Chemistry, Sapienza University of Rome, Piazzale Aldo Moro 5, Rome, 00185, Italy*
[c] *Department of Drug Science and Technology, University of Turin, Via Pietro Giuria, 9, 10125, Turin, Italy*
[d] *Institute for the Structure of the Matter (ISM), Italian National Research Council (CNR), Via del fosso del Cavaliere 100, 00133, Rome, Italy*

ARTICLE INFO

ABSTRACT

In the evolving field of nanomedicine, tailoring the mechanical properties of nanogels to fine-tune their biological performance is a compelling avenue of research. This work investigates an innovative method for modulating the stiffness of hyaluronan-cholesterol (HACH) nanogels, an area that remains challenging. By grafting dopamine (DOPA) onto the HA backbone, characterized through UV, ^{1}H NMR, and FT-IR analyses, we synthesized a novel polymer that spontaneously forms nanogels in aqueous environments. These HACH-DOPA nanogels are characterized by their small size (~170 nm), negative charge (around −32 mV), high stability, efficient drug encapsulation, and potent antioxidant activities (measured by ABTS test). Leveraging mussel-inspired metal coordination chemistry, the DOPA moieties enable stiffness modulation of the nanogels through catechol-Fe^{3+} interactions. This modification leads to increased crosslinking and, consequently, nanogels with a significantly increased stiffness, as measured by atomic force microscopy (AFM), with the formation of the HACH-DOPA@Fe^{3+} complex being pH-dependent and reversible. The cytocompatibility was evaluated *via* WST-1 cell proliferation assays on HUVEC and HDF cell lines, showing no evident cytotoxicity. Furthermore, the modified nanogels demonstrated enhanced cellular uptake, suggesting their substantial potential for intracellular drug delivery applications, a hypothesis supported by confocal microscopy assays. This work not only provides valuable insight into modulating nanogel stiffness but also advances new nanosystems for promising biomedical applications.

1. Introduction

In the realm of nanomedicine, the dimensions, morphology, surface characteristics, and other physicochemical parameters of nanoparticles have been extensively studied. These aspects' effects on drug delivery systems, especially for anticancer agents, have been systematically investigated [1–4]. However, tailoring the mechanical properties of nanocarriers for enhancing drug delivery has emerged as a burgeoning area of interest; recently, it has been recognised to play an important role in regulating their biological performances. This is mainly inspired by the fact that many cells or even viruses can modulate their mechanical properties to achieve certain biological functions [5,6]. Stiffness, a material's inherent resistance to deformation upon external

forces, is widely employed to characterise biological specimens, such as erythrocytes and cancer cells [7,8].

Despite accumulating evidence underscoring the pivotal role of material stiffness in biological contexts, a definitive consensus on the correlation between nanocarrier stiffness and their resultant biological fates remains elusive due to divergent findings in various studies [9,10]. Most studies suggest that soft particles exhibit extended blood circulation time compared to their stiff counterparts, which can be attributed to the superior deformability that enables them to elude phagocytosis by macrophages more effectively [8,9]. Moreover, this characteristic also contributes to the improved biodistribution and tumour accumulation observed with soft nanomedicines, likely resulting from their prolonged residency in the circulatory system. However, the arrival of

---

nanomedicines at a pathological site, such as tumour tissue, is not the end of drug delivery; on the contrary, it is just another beginning [11]. Nanomedicines need to penetrate and be internalised effectively by cells to exert a therapeutic effect after the long journey of blood circulation and their subsequent accumulation.

Therefore, great efforts have been dedicated to exploring the design principles of nanocarriers with enhanced cellular uptake. Numerous relevant studies claim that cancer cells prefer stiff nanomedicines over soft counterparts; the stiff particles display enhanced uptake by tumour cells, thereby promoting antitumor effectiveness [10,12,13]. While soft nanomedicines possess advantages in terms of blood circulation, accumulation, and penetration, stiff nanoparticles offer distinct benefits by enhancing cell association, which is crucial for intracellular drug delivery and situations where swift cellular internalisation is desired. For instance, stiff nano-vaccines administered intramuscularly have been shown to elicit improved immune responses, significantly affecting lymphatic transport and antigen presentation [14], as well as maintaining longer post-injection retention than their soft counterparts [15]. Furthermore, the topical *in-situ* administration of stiff nanomedicines emerges as another promising strategy for effective cancer treatment, in which injectable nanogels have received substantial interest for their delivery capabilities.

Polysaccharide-based nanogels have generated significant interest for their application in drug delivery, especially for overcoming biological barriers, owing to their excellent biocompatibility, biodegradability, and high drug-loading capabilities [16–19]. Among them, hyaluronic acid (HA), composed of alternately linked disaccharide units of glucuronic acid and *N*-acetylglucosamine *via* β-1,4- and β-1,3-glycosidic bonds, has gained prominence due to its inherent ability to target the CD44 receptor specifically, thus attracting considerable attention as a promising carrier for therapeutic agents [20–22]. Our previous work investigated the self-assembly process of injectable nanogels derived from cholesterol (CH)-modified HA, in which the incorporation of hydrophobic cholesterol moieties facilitated the transformation of the amphipathic polymer into nanogels in an aqueous environment through hydrophobic interactions. This nanosystem exhibited effective CD44-mediated intracellular drug delivery [23]. However, despite the promising outcome, a clear understanding of how modulations in the stiffness of these nanogels influence their biological efficacy remains an open question.

Two conventional strategies for modulating hydrogel stiffness include the variation of cross-linking density and the modification of hydrogel constituents [24]. However, modulating the stiffness of soft nanogel systems, such as the above-mentioned HACH nanogels, remains a substantial challenge. Over the past two decades, hydrogel systems inspired by the self-healing properties of mussel byssal threads have solicited great interest [25–27]. These hydrogel systems are based on the reversible metal-ligand coordination interactions between catechol-containing 3,4-dihydroxyphenylalanine (DOPA) groups and ferric iron. The combination of catechol and iron chelation imparts enhanced hardness and extensibility to these hydrogel systems and exhibits pronounced pH sensitivity [28,29]. Recently, several studies have reported catechol-functionalized HA derivatives that form hydrogels through iron-induced coordination crosslinking. Nevertheless, these investigations have predominantly focused on bulk systems with high polymer concentrations [30–33]. To our knowledge, there have been no reports about stiffness modulation of soft nanogels with low polymer concentration *via* catechol-iron coordination interactions.

In this study, we explore the tunability of the mechanical prosperities of soft HACH nanogels through the innovative use of mussel-inspired Fe^{3+}-catechol coordination interactions. Specifically, we reported the surface chemical modification, preparation, and characterization of the injectable HACH nanogels by inducing catechol groups. Additionally, the Fe^{3+} ions were utilised to modulate the stiffness of soft nanosystems, enhancing their internal crosslinking strength through multiple interactions, including coordination linkage, hydrogen bond and

electrostatic interactions. The morphology and nanomechanical properties of the nanogels were investigated through atomic force microscopy (AFM). We also evaluated their drug encapsulation efficiency, antioxidant activity, and biocompatibility. Crucially, we investigated how the stiffness of the nanogels affects their cellular internalisation behaviours on CD44-expressing cell lines. Overall, this study provides valuable insight into the stiffness modulation of soft nanogels and contributes to the advancement of new nanosystems with significant potential for application in drug delivery.

2. Materials and methods

2.1. Materials

2.1.1. Chemicals and materials

Hyaluronan-cholesterol (HACH, HA MW = 220 kDa, DF of CH = 11.3 %), S.N. 01-080222/dB, was provided by NOVAGENIT SRL, Trento. 1-(3-(Dimethylamino) propyl)ethylcarbodiimide hydrochloride (EDC·HCl), N-Hydroxysuccinimide (NHS), 2-(N-morpholino)ethanesulfonic acid (MES), dopamine hydrochloride, betamethasone, 2,2′-azino-bis (3-ethylbenzothiazoline-6-sulfonic acid (ABTS), acetone, acetonitrile (HPLC grade), phosphate buffered saline tablets (PBS), Ethylenediaminetetraacetic acid disodium salt dihydrate (EDTA-Na$_2$, ≥97 %), (3-aminopropyl)-triethoxysilane (APTES), petri dishes and dialysis tubing cellulose membrane were purchased from Sigma-Aldrich (Milan, Italy). Iron(III) chloride hexahydrate was purchased from Thermo Scientific Chemicals.

2.1.2. Cell culture

Two different human cell lines, umbilical vein endothelial cells (HUVEC, MERCK, Milano, Italy) and dermal fibroblasts (HDF, ECACC, Salisbury, UK), were considered as characterized by a high level of CD44 expression [34]. HUVEC were cultured in Endothelial Cell Growth Medium 2 (ECGM2, PromoCell, Milano, Italy) supplemented with the Supplement Mix (PromoCell) according to the manufacturer's instruction and HDF in DMEM-F12 (Dulbecco's Modified Eagle's Medium, Sigma-Aldrich) supplemented with fetal bovine serum (FBS 10 %, Sigma Aldrich), streptomycin (100 μg/mL, Sigma-Aldrich) and penicillin (100 units/mL, Sigma-Aldrich). Both cell lines were maintained in a humidified atmosphere of 5 % CO$_2$–95 % air at 37 °C and were used, in their first ten passages, for testing the cytotoxicity and cellular internalisation of the different nanogels.

2.2. Synthesis and preparation of HACH NHs

The method for the synthesis of hyaluronan-cholesterol (HACH) derivative was already described in detail in previous work [35]. The derivatisation degree of this amphipathic derivative is around 11.3 %, which is poorly soluble in water. However, it can form nanohydrogels/nanogels (NHs) by self-assembling HACH molecules.

HACH NHs were prepared before the synthesis to further modify HACH molecules, which allows for as much exposure as possible to the reaction mixture. Briefly, 50 mg of HACH was dispersed in distilled water (2 mg/mL) by magnetic stirring overnight at room temperature (RT). For NHs formation, the HACH suspension was then placed in an autoclave and a standard sterilising cycle was performed (121 °C, 1.1 bar, 20 min).

2.3. Synthesis of DOPA-modified HACH

Dopamine (DOPA)-modified HACH NHs were synthesized using EDC as an activation agent of the carboxyl groups on HA chains following a procedure already reported previously with some modification, where the carboxylic acid groups of HA were substituted with the amine groups of dopamine [33]. In a typical synthesis, 25 mL of HACH NHs (50 mg of polymer) was mixed with 2.5 mL of 0.5 M of 2-(N-morpholino)-

ethanesulfonic acid (MES) buffer (pH 4.8, final concentration around 50 mM) to adjust the pH of polymer suspension. 42.2 mg of EDC and 25.4 mg of NHS were then added and magnetic stirred for 30 min, followed by 41.8 mg of dopamine hydrochloride. All the stock solutions were prepared in 50 mM MES buffer (pH 4.8), and the molar ratio of reactants was -COOH groups of HACH: dopamine: EDC: NHS = 1:2:2:2. The pH of the mixture solution was maintained between 4.5 and 5.0 by adding 1 M HCl or 1 M NaOH. Afterwards, the solution was purged with nitrogen and kept nitrogen protected during the reaction under magnetic stirring at 25 °C overnight. Then, the solution was dialysed against a pH ~5 aqueous solution for 2 days, followed by dialysing again in distilled water for 8 h to fully remove unreacted reagents and salts (membrane molecular weight cutoff between 12,000–14,000 Da). The synthetic polymer of HACH-DOPA was obtained by lyophilising the resultant solution. The catechol modification of HACH-DOPA was confirmed by UV, FTIR and ^{1}H NMR.

2.4. Synthesis of fluorescence-labeled NHs

Fluorescent HACH (Rhod-HACH) or HACH-DOPA (Rhod-HACH-DOPA) were synthesized as previously reported with some modifications [23,36]. Briefly, 1 mg/mL of HACH or HACH-DOPA polymers were dispersed in bi-distilled water under magnetic stirring for 5 h at room temperature. Subsequently, the HACH suspension underwent autoclaving (121 °C for 20 min), and the HACH-DOPA suspension underwent sonication in the water bath for 30 min to enable the self-assembly of NHs. Ferric chloride (4 mM in water) was used to protect catechol groups of HACH-DOPA polymers by coordination reaction before the synthesis with Rhodamine B. Rhodamine B-isothiocyanate (Rhod) stock solution in DMSO (9 mg/mL) was added to HACH or HACH-DOPA NHs suspension (8 µL for 1 mg of polymers corresponding to a degree of functionalisation (DF) of 6.1 and 6.4 % for HACH and HACH-DOPA, respectively). The reaction mixtures were kept under magnetic stirring for 5 h at 25 °C in the dark. Subsequently, exhaustive dialysis against water was carried out. In the case of dialysing Rhod-HACH-DOPA, an equimolar concentration of EDTA was introduced into the dialysis water, and the pH was adjusted to approximately 5 using hydrochloric acid. This step aimed to remove the iron ions from the complex over the course of overnight dialysis, followed by further dialysis against water. Rhod-labeled polymers were obtained through freeze-drying and stored at 4 °C in the dark. Before using, Rhod-NHs were prepared by re-dispersing at a concentration of 1 mg/mL in bi-distilled water and sonicated for 30 min to allow the formation of NHs.

2.5. Characterization of HACH-DOPA derivatives

A Lambda 25 UV–Vis spectrophotometer (Perkin Elmer, US) was used to record the absorption spectra of the HACH-DOPA nanogels (1 mg/mL); the wavelength was in the range of 200–800 nm. Double-distilled water was used as a blank solution. In addition, to confirm the conjugation of catechol in the HACH, ^{1}H NMR spectra were collected on a JNM-ECZ 600R spectrometer and using D$_2$O as the solvent to obtain a final concentration of 10 mg/mL. The degree of functionalisation was calculated by comparison of the area of 6.5–7.5 ppm and 1.8–2.2 ppm peaks using the following Eq. (1):

$$DF\% = \frac{\frac{1}{3} \times \text{Area } (6.5 - 7.5 \text{ ppm})}{\text{Area } (1.95 \text{ ppm})} \times 100 \qquad (1)$$

Fourier transform infrared (FT-IR) spectra of HACH and HACH-DOPA samples were recorded at wavenumber region of 4000–650 cm^{-1} using an FTIR Cary 630 spectrometer equipped with ATR system (Agilent Technologies, Santa Clara, California, US).

To quantitatively assay dopamine non-covalently linked to the polymer chains, the lyophilised polymer was dispersed in methanol (MeOH) at the concentration of 1 mg/mL by magnetic stirring at 25 °C

for 5 h. The free dopamine dissolved in MeOH was measured by UV after separating the insoluble polymer *via* centrifugation at 3000 rpm for 15 min at 25 °C (Universal 30RF, Hettich Zentrifugen, Germany).

2.6. HACH-DOPA nanogels preparation and drug encapsulation

To produce nanogels, the HACH-DOPA lyophilised product was dispersed in distilled water (1 mg/mL) by magnetic stirring at RT for 5 h. For nanogel formation, the suspension was then sonicated for 30 min using an ultrasonic bath sonicator (Strasonic 18–35, Liarre).

Betamethasone was solubilised in acetone at the concentration of 2 mg/mL as the stock solution, and 0.5 mL of stock solution was added to a glass vial and allowed to evaporate by rotary evaporator (Buchi, Schwabach, Germany) in order to form the film of the drug, then mixed with 3 mL of nanogels. Afterwards, the mixture was kept under magnetic stirring at 25 °C overnight, followed by sonication in an ultrasonic bath sonicator for 20 min. Drug-loaded nanogels were obtained by centrifugation at 4000 rpm for 15 min at 25 °C (Universal 30RF, Hettich Zentrifugen, Germany).

2.7. Preparation of Fe^{3+}-induced modulation of nanogels

Fe^{3+} ions were mixed homogeneously with HACH-DOPA nanogels to modify the nano-system. To study the effect of Fe^{3+}: catechol ratio upon the interactions, iron (III) chloride hexahydrate solution of different concentrations (4 mM and 12 mM) was prepared in distilled water. 3 mL of nanogels were treated with 45 µL of 4 mM or 12 mM of Fe^{3+} ions to give a 3:1 or 1:1 of catechol: Fe^{3+} molar ratio. pH, particle dimension, zeta potential, and stiffness of nanogels were measured after the modulation of Fe^{3+}.

2.8. Dynamic light scattering (DLS)

Nanogel size, polydispersity (PDI), and ζ-potential of nanogels and Fe^{3+} treated nanogels were determined by DLS using a Zetasizer Nano ZS instrument (Model ZEN3690, Malvern Instruments, Worcetershire, UK) equipped with a solid state HeNe laser (λ = 633 nm) at a scattering angle of 173°.

To investigate the stability of HACH-DOPA nanogels and Fe^{3+} modified nanogels, DLS measurements were performed, samples were stored at 4 °C between the measurements, and each measurement was carried out at ambient temperature and in triplicate (*n* = 3).

2.9. Determination of drug encapsulation efficiency (E.E)

The drug loading efficiency was indirectly determined by quantifying the unloaded drug using HPLC. Briefly, a Knauer Azura HPLC instrument was used for the analysis, which was equipped with a binary pump (Azura P 6.1 L) and a UV–Vis detector (190–750 nm, Azura UVD 2.1 L), and controlled by Clarity software. Chromatographic conditions as follows: a Knauer Eurospher II C18 column (4.6 × 250 mm, 5 µm) was used for the separation; acetonitrile: water (50:50, *v/v*) as mobile phase, at initial isocratic mode, followed by gradient mode from 50:50 to 100:0; flow rate v = 1 mL/min, detection wavelength λ = 250 nm, 20 µL of the sample was loaded for each injection and analyses were performed at ambient temperature. The pellets of unloaded drug after centrifugation were solubilised in acetonitrile for quantitative analysis, using a calibration curve previously recorded with BM standard solution in acetonitrile in the range of 1–200 µg/mL (R^2 = 0.9999).

Encapsulation efficiency (*EE*) and drug loading (*DL*) were calculated by using the following Eqs. (2) and (3).

$$EE\% = \frac{(\text{Total mass of drug}) - (\text{Mass of untrapped drug})}{\text{Total mass of drug}} \times 100 \qquad (2)$$

$$DL\% = \frac{\text{Concentration of loaded drug}}{\text{Polymer concentration}} \times 100 \qquad (3)$$

2.10. Evaluation of the antioxidant activity

Antioxidant activity of HACH-DOPA nanogels and Fe^{3+} modified nanogels was evaluated by ABTS assay, as previously reported [37], using an HP8452A (Hewlett Packard, Palo Alto, CA, US) singular beam spectrophotometer working in the 190–820 nm wavelength range and with a resolution of 2 nm.

A solution (containing $ABTS^{\bullet+}$) was prepared and left overnight at 25 °C in the dark before use, by adding 88 μL of $K_2S_2O_8$ solution (38 mg/mL) in double-distilled water to 5 mL of ABTS solution (3.8 mg/mL) to allow free radical generation, corresponding to a molar ratio of 2.3 (mol of ABTS per mol of $K_2S_2O_8$). The mixture was then diluted ~1:80 with double-distilled water in order to have an absorbance (Abs) of 0.70 ± 0.02 at 730 nm.

Afterwards, 0.1 mL of nanogel (1 mg/mL) sample was added to 2.9 mL of diluted $ABTS^{\bullet+}$ solution and the Abs were monitored at $\lambda = 730$ nm at different time points (from 0 to 20 min). For an appropriate comparison, the ABTS assay was tested on DOPA (40 μg/mL), dopamine-free HACH nanogels at the same concentration as well as the Fe^{3+} modified nanogels. The antioxidant activity (AA%) was calculated, by using the following Eq. (4):

$$AA\% = \frac{\text{Abs (ABTS)} - \text{Abs (Sample)}}{\text{Abs (ABTS)}} \times 100 \qquad (4)$$

2.11. Atomic force microscopy (AFM) measurements

AFM measurements were performed with a PARK NX12 microscope (Park Instruments, Korea) mounted over a Nikon Eclipse Ti2 inverted optical microscope (Nikon, USA). For each measurement, mica substrates (with dimensions of 1.0 cm × 1.0 cm) were placed in a petri dish and chemically functionalized by drop-casting of 50 mL of APTES for 10 min, to favour the absorption of the NHs, followed by cleaning of the excess APTES with ultrapure distilled water. An aliquot of 50 mL of the sample was deposited on the functionalized mica and left in adhesion for at least 8 h at 4 °C.

Before inserting the sample in the AFM, the petri dish bearing the mica substrate with the sample was gently filled with 3 mL of ultrapure distilled water to ensure the hydration of the specimen throughout the measurements. The measurements were performed firstly in non-contact mode to obtain a high-resolution image of the area and subsequently using a fast force-volume modality (Pin-Point) to determine the elastic properties of the specimens. In both cases, we used silicon nitride qp-BioAC (Nanosensors, Switzerland) tips, with nominal elastic constant and resonant frequency of 0.03 N/m and 37 kHz, respectively. To ensure optimal control over the force exerted by the AFM tip on the sample, before the analysis of each sample, the elastic constant of the tip was measured using the built-in thermal noise method. The high-resolution images were acquired using at least 512 × 512 points and with a 30 % damping rate. The Pin-Point data contained no <64 × 64 force curves each and were acquired using a maximum applied force of 2 nN. All samples were analysed in at least 9 different areas and all the experiments were performed in triple independent preparations.

2.12. Cell proliferation assay

The effect of nanogels and Fe^{3+} modified nanogels on cell proliferation was evaluated by WST-1 cell proliferation assay (Roche Applied, Sigma Aldrich). Briefly, cells were seeded in 96 well plates at a density of 1000 and 2000 cells per well for HUVEC and HDF, respectively. Two days after the seeding, cells were incubated with increasing concentrations of HACH-DOPA or HACH-DOPA@Fe^{3+} nanogels (10, 50, 100, 150, and 250 μg/mL), and HACH nanogels (250 μg/mL). Furthermore, untreated cells were considered as a control. The evaluation of cell proliferation was performed on both HUVEC and HDF cells by WST-1 reagent (Sigma Aldrich) that was added to each well (10 μL/100 μL) at 24, 48, and 72 h, and the plates were incubated at 37 °C in 5 % CO_2 for 4 h. The absorbance of the well was measured at 450 and 620 nm (reference wavelength) in a microplate reader (Asys UV340, Biochrom, Cambridge, UK).

2.13. Cell uptake evaluation of fluorescently labeled nanogels

Thirty thousand HUVEC and HDF cells were seeded, respectively, in 6-well culture plates and allowed to a growth for 72 h before the treatment. Subsequently, Rhod-labeled NHs or Fe^{3+}-modified labeled NHs were added to the cell culture medium at an appropriate concentration of 100 μg/mL and incubated for 5 and 24 h at 37 °C within an incubator with 5 % CO_2. After the incubation period, cells were detached using a 0.05 % trypsin-0.02 % EDTA solution, the pellet was centrifuged and resuspended in 200 μL of PBS. The cytofluorimetric analysis of the intracellular nanoparticles was conducted using flow cytometry (Accuri C6, Milano, Italy), with excitation at 488 nm by considering 10,000 events and medium flow rate and by discarding cellular debris, with low forward scatter (FSC) and low side scatter (SSC) from the analysis. The integrated mean fluorescence intensity (iMFI), which is the product of the frequency of Rhod-positive cells and the mean fluorescence intensity of the cells, was used to express the internalisation, which is the ratio between the iMFI values of the treated and untreated cells.

2.14. Confocal microscopy evaluation of fluorescently labeled nanogels

Twenty thousand HUVEC and HDF cells were seeded in 24-well plates with glass coverslips on the bottom of the wells and allowed to a growth for 72 h before the treatment. Subsequently, Rhod-labeled NHs or Fe^{3+}-modified labeled NHs were added to the cell culture medium at an appropriate concentration of 100 μg/mL and incubated for 5 h and 24 h at 37 °C within an incubator with 5 % CO_2. After the incubation period, cells were washed with PBS and then incubated with Lyso-Tracker Green (Life Technologies) 60 nM for 90 min at 37 °C, in the last 15 min of incubation a solution of 4′,6-diamidino-2-phenylindole (DAPI, Sigma-Aldrich) was added to stain cell nuclei for 15 min at 37 °C. When the incubation was finished, all slides were washed twice with PBS and then fixed with paraformaldehyde (PAF, 4 %) for 15 min at room temperature. Finally, the slides were then washed again, and glass coverslips were placed on the slides with Fluoroshield™ mounting medium (Sigma-Aldrich, Milano, Italy) to preserve the cells and prevent the rapid photobleaching of the fluorescent probe. Confocal images were acquired using a laser scanning confocal microscope (LSM 900, Zeiss, Milano, Italy) with a 40× oil immersion objective using the multitrack mode.

2.15. Statistical analyses

For the experiments, statistical significance was determined by using a one-way analysis of variance (ANOVA) with GraphPad Prism 9.5.1 Software (Graph Pad Software Inc., La Jolla, CA, USA). Differences between groups were determined by Tukey's multiple comparison test. For the AFM results, the stiffness and size of the structures were analysed using a one-way analysis of variance (ANOVA) using Origin Pro (OriginLab, USA). All results are presented as mean ± standard deviation (SD). Asterisks denote statistically significant differences. The level of statistical significance was set to a p-value <0.05.

3. Results

3.1. Synthesis and characterization of HACH-DOPA

The amphipathic polymer of HACH (DF 11.3 %), which has been developed and described in previous papers, was chosen as raw materials for further modification [23,36]. To obtain catechol-modified HACH, dopamine moieties were grafted onto the HACH backbone, which endows the structural component for tunable properties. EDC and NHS were added to the reaction system to activate the carboxylic groups of HACH, thereby enabling the coupling of polymer with the amino group of dopamine moieties. The reaction formula is shown in Fig. 1A.

UV spectroscopy, FT-IR spectra, and ^{1}H NMR were employed to demonstrate the successful grafting of dopamine on the HACH backbone and evaluate the degree of functionalised substitution. The catechol group of dopamine gives an absorption peak at 250–300 nm in a pure water environment, while HACH does not. As shown in Fig. 1B, S1,

maximum absorption peaks at 280 nm are shown both in the standard dopamine and physical mixture with unmodified polymer samples, while the absorption peak of modified polymer exhibits a slight blue shift (at 275 nm) probably because of the influence of the N-substituent group (HACH molecule) of DOPA, indicating the grafting of dopamine onto the HACH backbone. To further demonstrate the modification of dopamine by means of chemical linkage, the modified polymers were suspended in MeOH to extract the free dopamine (non-covalent linkage), since the polymers are insoluble in MeOH. The results indicated that the amount of non-covalent linkage of dopamine in HACH-DOPA polymers was much lower than 2.5 µg in each milligram of polymer, which was lower than the limit of quantitation of the calibration curve (Fig. 1C).

The successful synthesis of HACH-DOPA was also confirmed by ^{1}H NMR. As shown in Fig. 1D, proton peaks for the DOPA group (6.5–7.5 ppm) were observed in the ^{1}H NMR spectrum, and the content of DOPA in synthesized HACH-DOPA analysed by ^{1}H NMR was 11.2 %. The
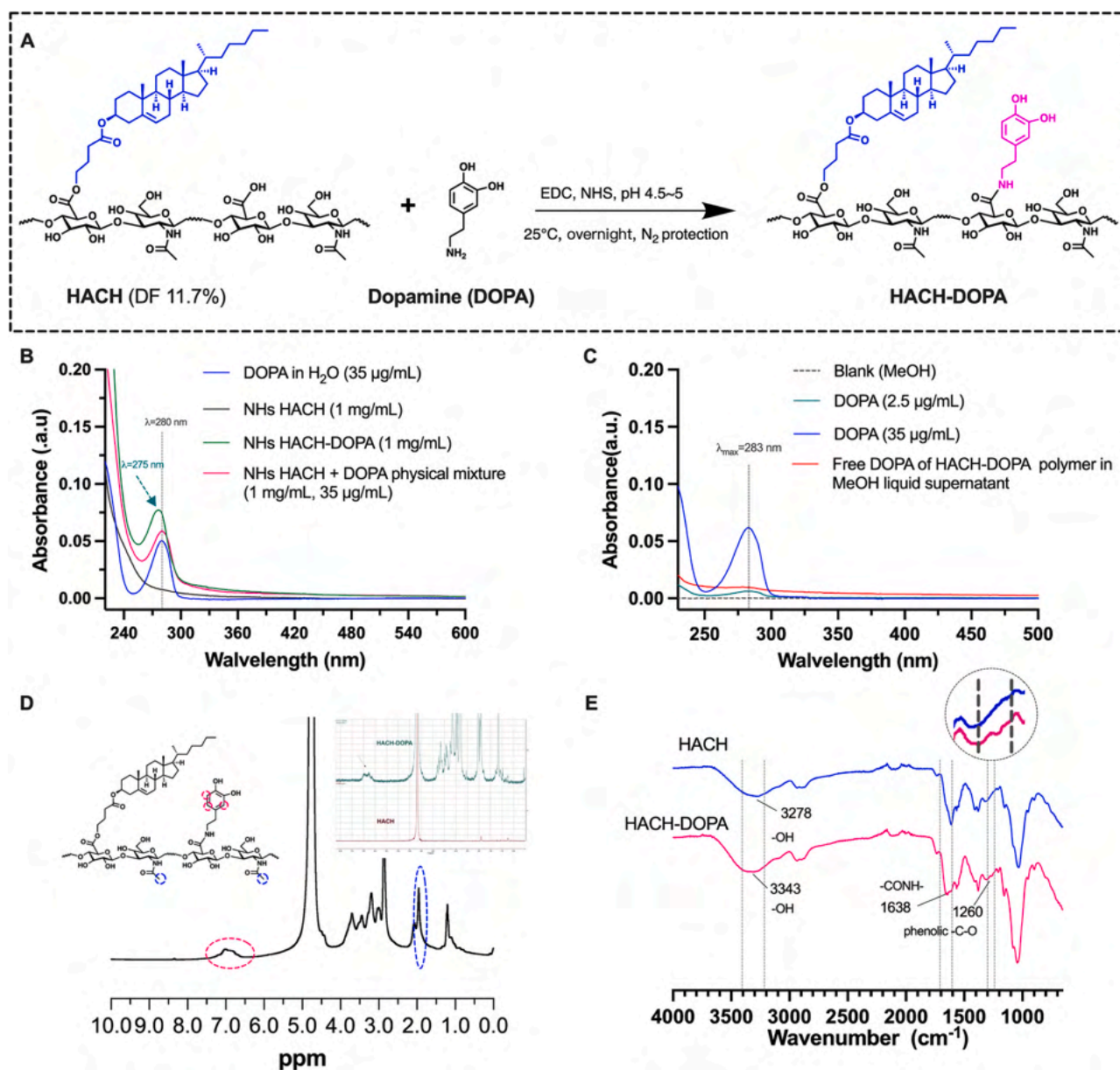

Fig. 1. (A) Schematic process of the catechol-modified HACH (HACH-DOPA); (B) UV–visible spectra of HACH-DOPA, HACH, DOPA, and their physical mixture in water; (C) quantitative analysis of non-covalent linkage of dopamine in the modified polymer, measuring by the precipitation of polymer in MeOH solution with a concentration of 1 mg/mL; (D) ^{1}H NMR spectra and (E) FTIR spectra of HACH and HACH-DOPA polymers.

calculation was performed using the area of methylene of catechol moieties (6.5–7.5 ppm) and methyl of HA (1.95 ppm) based on the formula outlined in Section 2.5. Integral ratios were obtained using the MestReNova software (version 14.3.2), and the calculation method can be found in Fig. S2.

In the FT-IR spectrum (Fig. 1E), both spectra show a broad peak at 3200–3400 cm^{-1} that corresponds to the stretching of –OH and –NH groups [38]. Notably, the difference in peak intensity of HACH-DOPA compared with that of HACH may be due to the co-existence of these groups in the chemical structure of dopamine. The new characteristic peak at 1638 cm^{-1} in HACH-DOPA may be assigned to the amide bond between HACH and dopamine [39]. Moreover, the HACH-DOPA spectrum displays a characteristic peak at 1260 cm^{-1} that is not present in the spectrum of unmodified HACH (magnification in Fig. 1E), which can be assigned to the C—O single bond vibration of phenolic moieties [40]. Overall, the FT-IR characterization of the HACH-DOPA indicates the presence of grafted dopamine moieties, in line with the UV–visible and ^{1}H NMR analyses. These results provided evidence for the successful conjugation of HACH with DOPA.

3.2. Preparation, characteristics, and stability of nanogels

In the previously reported studies, the sterile HACH nanohydrogels or nanogels (NHs) were synthesized relying on the self-assembly in water under the condition of autoclave, in which the CH moieties contribute to form a hydrophobic core and the hydrophilic HA chains expose to the solvent, as is shown in Fig. 2A [23,36]. In this study, we further modified the amphipathic system by inducing dopamine moieties; however, the catechol group of dopamine is prone to oxidation

under harsh conditions. The novel HACH-DOPA nanogels were prepared by bath-sonication in aqueous media at the concentration of 1 mg/mL following the procedure already described for the HACH polymer system [41]. Similarly, for the HACH polymer system, the self-assembly of amphiphilic HACH-DOPA in the aqueous environment is mainly due to the hydrophobic interactions among the hydrophobic core-forming cholesterol moieties and hydrophilic HA chains as well as the dopamine moieties. In addition, the dopamine-modified polymer is rich in benzene rings and phenolic hydroxyl groups. Thus, there were also a large number of hydrogen bonds and π–π stacking effects in the nano-hydrogel network (shown in Fig. 2B), accounting for the ease of formation of nanogels as well as the versatile functionalisation.

The size of the obtained HACH-DOPA nanogels was smaller than that of HACH nanogels prepared under the same conditions. The size decreased by increasing the sonication time up to 30 min; thereafter, it remained almost unchanged. The stability of the nanogels, investigated at 4 °C, showed that HACH-DOPA nanogels are stable in aqueous media for at least 35 days, as reported in Fig. 3, whereas the HACH nanogels prepared with the same conditions showed slightly larger size and higher PDI, although have the similar stability.

We investigated the capacity of HACH-DOPA nanogels to encapsulate betamethasone (BM), a hydrophobic steroid drug. To obtain drug-loaded nanogels, a mixture of 3 mL of nanogels and 1 mg of BM was prepared and subjected to sonication treatment. The results indicated that this novel nano-system enabled an effective encapsulation of BM and, to some extent, demonstrated superior drug encapsulation capability compared to HACH nanogels. As is shown in Fig. 4A, the encapsulation efficiency (EE%) of HACH-DOPA nanogels (41.1 ± 5.4 %, $n = 5$) is higher than that of HACH nanogels (34.4 ± 6.6 %, $n = 4$),
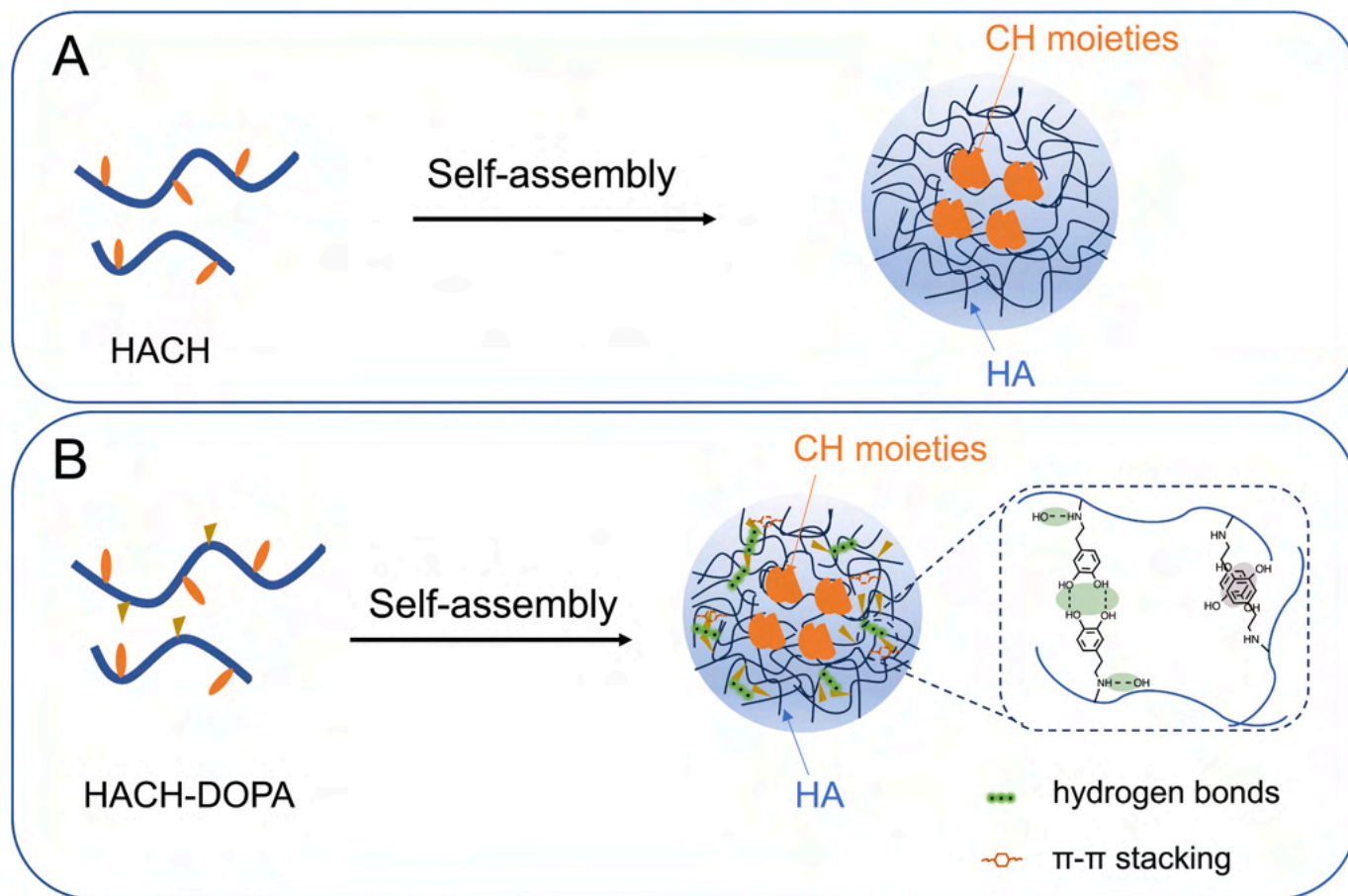

Fig. 2. Schematic illustration of (A) HACH nanogels formed by hydrophobic interactions and (B) HACH-DOPA nanogels formed by the association of hydrogen bonding and π–π stacking except for hydrophobic interactions.
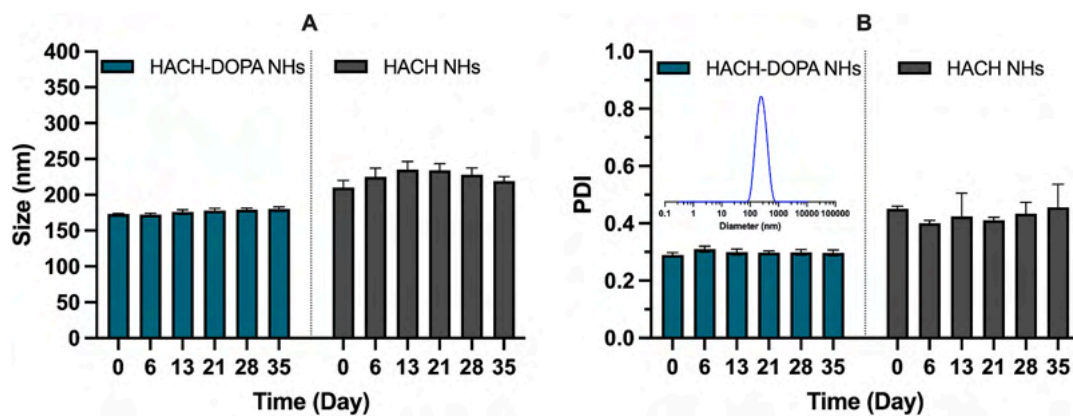
Fig. 3. The stability of nanogels at a concentration of 1 mg/mL in water: (A) mean dimension and (B) PDI, representative graph of size distribution for HACH-DOPA nanogels. All data are presented as mean value ± standard deviation. Each measurement was done in triplicate ($n = 3$).
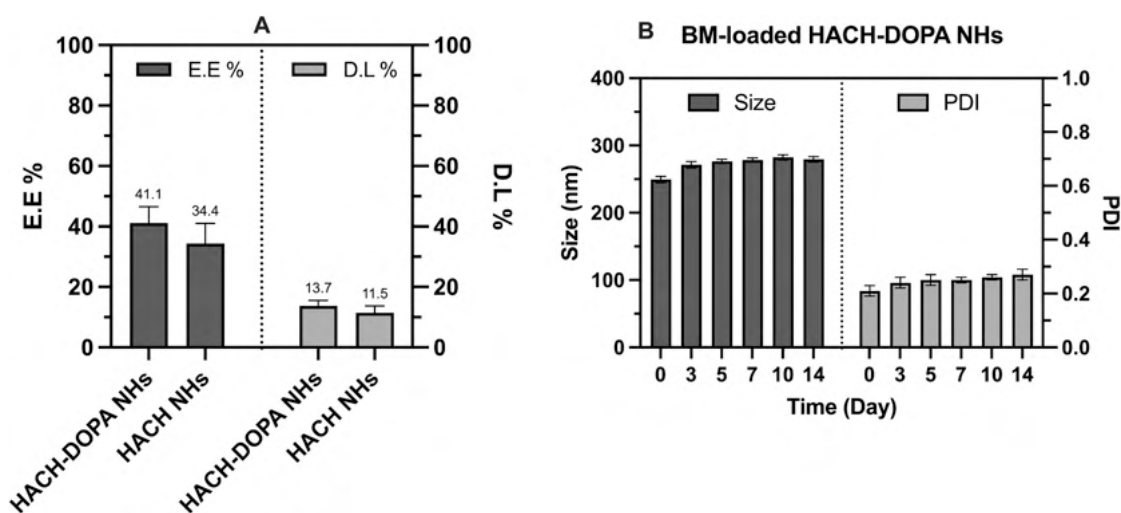

Fig. 4. (A) EE% and DL% of HACH-DOPA nanogels, with HACH nanogels as the control; (B) Mean diameter and PDI of drug-loaded HACH-DOPA nanogels as a function of the time at 4 °C. All the data are expressed as the mean value ± standard deviation. Results were obtained at least in triplicate.

corresponding to drug loading (DL%) by polymer weight 13.7 ± 1.8 % and 11.5 ± 2.2 %, respectively. The drug encapsulation ability of HACH nanogels has been investigated in previous work, demonstrating excellent drug-loading efficiency under autoclave conditions for hydrophobic molecules [36]. Here, drug encapsulation under sonication conditions can serve as a reflection of the drug-loading properties of the nanogels. The slightly higher EE and DL of HACH-DOPA nanogels can be attributed to multiple physical interactions, such as hydrogen bonds and π-π stacking, facilitated by the dopamine moieties in the nanogel system. The average concentration of BM in the HACH-DOPA nanogels was 137 ± 18 μg/mL, which showed an enhanced apparent solubility by more than two times [42]. Besides, the stability of drug-loaded nanogels was investigated, and they were almost stable for at least two weeks at 4 °C (Fig. 4B).

3.3. Characterization of nanogels modulated with Fe^{3+} via coordination bonds

To modulate the properties of dopamine-modified nanogels, the tunable stiffness of the nanogel system was constructed by mussel-inspired catechol-Fe^{3+} coordination bonds. The catechol groups possess fascinating chelating potential owing to the complex formation of catechol with Fe^{3+}. In the present work, a certain amount of $FeCl_3$ solution was directly added to HACH-DOPA nanogels or drug-loaded nanogels with a molar ratio of 3:1 between the catechol group and

Fe^{3+}. Interestingly, the formation of complex aroused instantaneously when the HACH-DOPA nanogels containing Fe^{3+} ions, as the colour of the system changed from colourless to pale green immediately when 37 μL of 4 mM ferric ion solution was added to 3 mL of HACH-DOPA nanogels, whereas there was no colour change occurred for the HACH nanogels system. Notably, compared with other physical interactions, the coordination bonds between catechol and Fe^{3+} are remarkably strong and are closer to covalent bond binding energy [43]. More importantly, the negatively charged carboxylate group in the HA backbone allows electrostatic interactions between Fe^{3+} and carboxylate. Therefore, the catechol-Fe^{3+} complex may impart good mechanical strength and stability to HACH-DOPA nanocarriers by providing tighter intramolecular and/or intermolecular interactions. Indeed, as is shown in Fig. 5, the introduction of Fe^{3+} in the HACH-DOPA system led to a significant decrease in size without obvious influence on PDI, indicating that the catechol-Fe^{3+} complex gives tighter interactions in the nanogels system. Furthermore, the net values of zeta potential decreased significantly after the formation of the catechol-Fe^{3+} complex due to the electrostatic interaction (Fig. 5C).

A similar phenomenon was observed in the drug-loaded HACH-DOPA nanogels system. However, there was no obvious influence on the HACH nanogel system when introducing ferric ions (Fig. 5D-F). Therefore, Fe^{3+} is unable to significantly modify the properties of HACH nanogels. Moreover, the stability of Fe^{3+} modified both HACH-DOPA nanogels and drug-loaded HACH-DOPA nanogels were investigated by
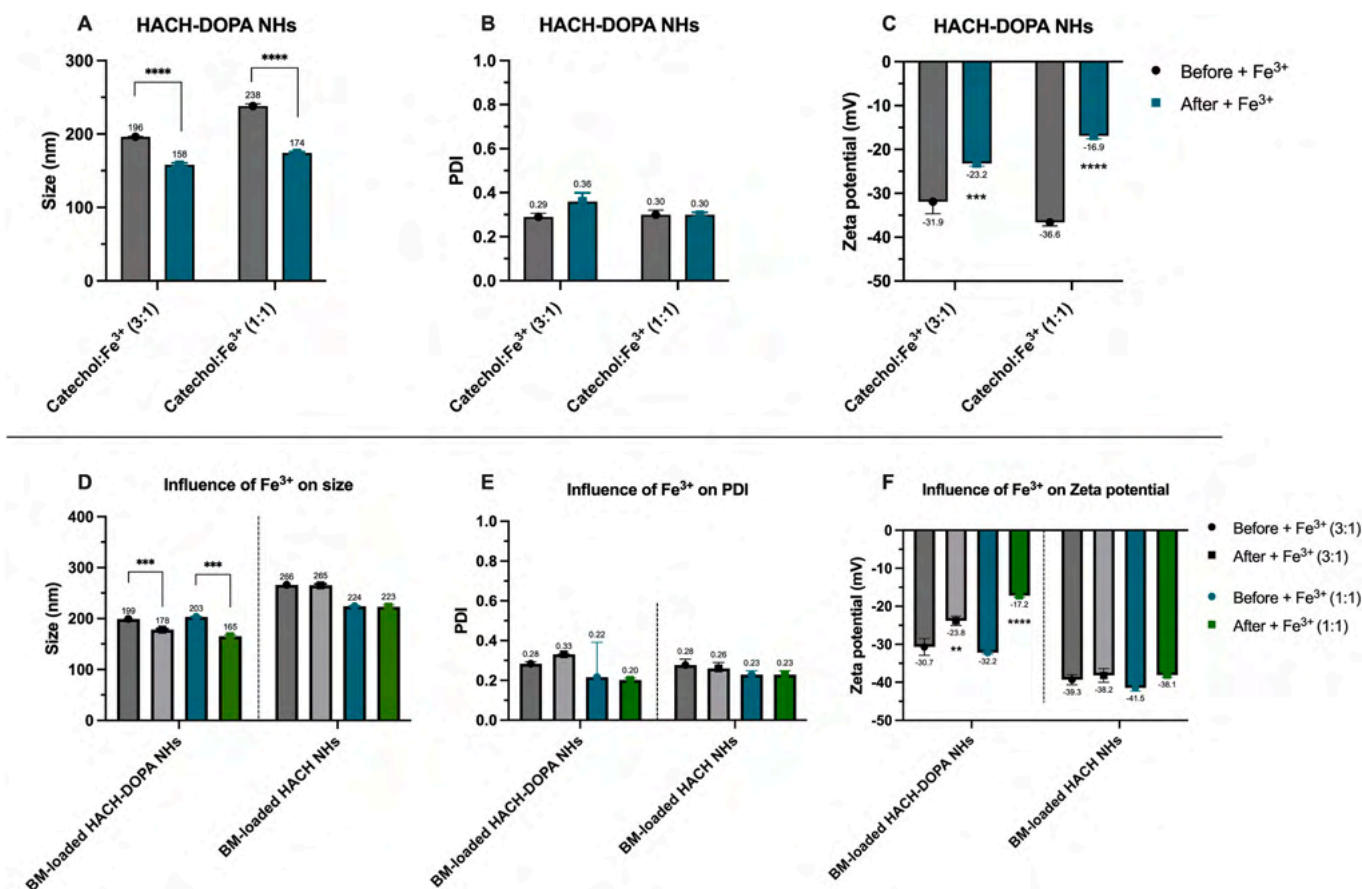
Fig. 5. The influence of introducing Fe^{3+} on (A, D) size, (B, E) PDI, and (C, F) zeta potential of HACH-DOPA nanogels (A-C) and drug-loaded HACH-DOPA nanogels (DL% ~15 %) (D-F), drug-loaded HACH nanogels as the control. The different molar ratios (3:1 and 1:1) between the catechol group and Fe^{3+} were investigated. All data are presented as mean value ± standard deviation. Results were obtained in triplicate (n = 3), * $p < 0.05$, ** $p < 0.01$, *** $p < 0.001$, **** $p < 0.0001$.

DLS analysis, as is shown in Fig. 6; there were no obvious changes in size and PDI, indicating all the samples are stable in refrigerator storage for >4 weeks.

3.4. Effect of pH on coordination interaction and Nanogel system

As previously well investigated, the mussel foot secretion has been proposed at acidic pH (~5–6) [44,45], the Fe^{3+} is prebound in DOPA-Fe^{3+} mono-complexes by mfp-1 in secretory granules at pH ≤ 5. When it is exposed to seawater, the significant pH jump and rapidly equilibrate to alkaline marine would cause nascent thread cuticle material to undergo a spontaneous cross-linking process *via* the formation of bis- and/

or tris-DOPA-Fe^{3+} complexes [29]. Generally, the metal coordination interaction between catechol and iron ions is strongly dependent upon the pH of the solution and has been described in other works [29,46,47]. The above experiments were all performed under acidic conditions, as the pH of HACH-DOPA nanogels in water revealed around 4.5. As a result, the pale green mono-complexes formed at the catechol- Fe^{3+} ratio of 3:1. However, the results demonstrated that the change in catechol-Fe^{3+} ratio would affect the coordination effect, the mono-complexes were more prone to form at the ratio of 3:1 than that of 1:1, the spectroscopic evidence is shown in Fig. S3, which is consistent with the results reported by Shubin Li et al. [48]. Therefore, considering the applications of nanogels, we focused on the formation of complexes at
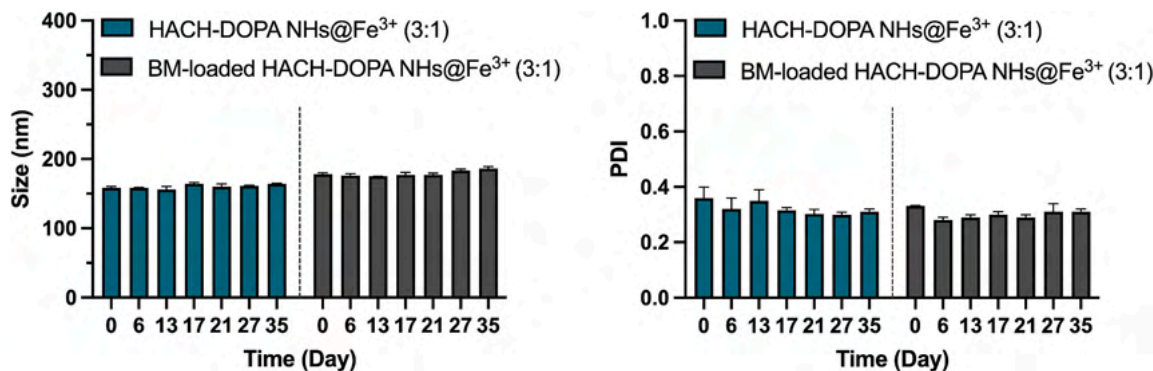

Fig. 6. The mean diameter and PDI of Fe^{3+} modified HACH-DOPA nanogels and drug-loaded nanogels (DL% ~15 %) as a function of time at 4 °C. All the data are expressed as the mean value ± standard deviation. Results were obtained in triplicate (n = 3).

the catechol-Fe^{3+} ratio of 3:1 and investigated the influence of pH on the coordination effect from acidic to physiological conditions.

As shown in Fig. 7, the initial HACH-DOPA@Fe^{3+} complex of HACH-DOPA nanogels at a concentration of 1 mg/mL modified with $FeCl_3$ at a molar ratio of 3:1 between the catechol group and Fe^{3+} yielded a UV–visible spectrum with a wide peak at 600-800 nm, which demonstrates the formation of mono-complex dominates at initial pH (~4.3). Besides, a similar UV absorption behaviour was observed when the pH was adjusted to 5.1 with 0.05 M of NaOH (Fig. 7). With a further pH increase to 7.4, the peak showed a clear shift to 450-600 nm. At the same time, the colour of the system changed from pale green to purple-blue. This phenomenon is attributed to the stoichiometry of catechol-Fe^{3+} transforming successively from mono-to bis-complex with increasing pH values, which is in good agreement with the expected coordination behaviour presented in Fig. 8 and with previous results presented by Menyo et al. [47]. To investigate the reversibility of the nanogel system, the nanogel@Fe^{3+} complex with pH 7.4 was recovered to pH 5.0 by adding 0.05 M HCl. Interestingly, as is shown in Fig. 7A and Fig. S4, the UV absorption characteristic is similar to that of the initial state; at the same time, the colour of nanogels recovered from purple to pale green, suggesting good reversibility of this nanogel@ Fe^{3+} complex system.

Moreover, the influence of pH on the properties of nanogels was also investigated, and the results indicated that the formation of mono-complex dominates led to a significant decrease of dimension without obvious change of PDI when compared with that of HACH-DOPA nanogels. More importantly, the size of nanogels decreased further following the formation of bis-complex dominates at pH 7.4 (Fig. 7B). Furthermore, the obvious influence of complex formation on zeta potential was observed due to the electrostatic interaction between Fe^{3+} and negatively charged nanogels. The net value of the zeta potential of the nanogels complex slightly increased when the pH increased from 4.5 to 7.4 (Fig. 7C) because of the decrease in the positive charge of Fe^{3+} when exposed to a nearly neutral environment.

3.5. Antioxidant activity of HACH-DOPA nanogels

After the preparation of HACH-DOPA nanogels and Fe^{3+} modified nanogels, the antioxidant activity of samples was evaluated by the spectrophotometric ABTS test (described in Section 2.9) in order to verify the existence of free catechol groups in the nano-systems. The test is based on the UV absorption (at 730 nm) of the stable radical $ABTS^{\bullet+}$ that is generated by a preliminary interaction in a solution of ABTS with $K_2S_2O_8$. By measuring the absorbance (Abs) after the introduction of a molecule with antioxidant activity, it is allowed to assess its effect on the decrease in Abs due to the conversion of $ABTS^{\bullet+}$ in its non-radical form $ABTS^+$.

It is known that compounds containing more phenolic hydroxyl groups have stronger antioxidant activity [49]; DOPA is recognised as an endogenous catechol antioxidant produced from nerve cells responsible for regulating brain functions [50]. Fig. 9A illustrates the trend of Abs of $ABTS^{\bullet+}$ when incubated with blank control, HACH nanogels, HACH-DOPA nanogels, and Fe^{3+} modified nanogels, in which the concentration of polymer was 1 mg/mL in water. As expected, both HACH-DOPA nanogels and HACH-DOPA@Fe^{3+} complexes exhibited significant antioxidant activity. However, the HACH nanogel did not show effective free radical scavenging properties; this significant difference in antioxidant activity demonstrated not only the successful introduction of DOPA onto HACH polymer but also the radical scavenging property being retained. Considering the decrease in Abs at 5 min and 24 h, the antioxidant activity (AA%) of samples was calculated according to Eq. (4) (Section 2.9). The results indicated that the HACH-DOPA nanogel displayed higher AA% (38.2 %) than that of HACH-DOPA@Fe^{3+} complexes at the same time point (5 min), with AA% of 33.6 % and 22.9 % for ratios of 3:1 and 1:1, respectively (Fig. 9B). The lower AA% of HACH-DOPA@Fe^{3+} complexes may be ascribed to the formation of coordinate bonds between catechol groups and Fe^{3+}, resulting in less phenolic hydroxyl group exposure to remove $ABTS^{\bullet+}$ radicals. Similarly, after incubation for 24 h, HACH-DOPA nanogel and HACH-DOPA@Fe^{3+} (3:1) complex achieved complete $ABTS^{\bullet+}$ radical scavenging, in comparison to the 1:1 ratio of Fe^{3+} complex while showing a 61.7 % of antioxidant activity.

3.6. AFM imaging and mechanical testing

AFM technique can study soft and stiff systems in air or liquid environments, with little need for sample preparation and no need for staining. Indeed, AFM is routinely employed in the study of samples of interest to biological and medical issues [51,52], often combined with other complementary techniques [53,54], with very interesting results at the single cell or molecule levels. In this sense, the ability to probe a single nanogel can provide a detailed overview of the different nanogel preparation protocols and allows for comparing the properties of the particles obtained through the various treatments [35].

AFM measurements were performed in ultrapure water with the nanogels immobilised on a mica substrate. The morphology measurements were performed in non-contact mode, while the stiffness data
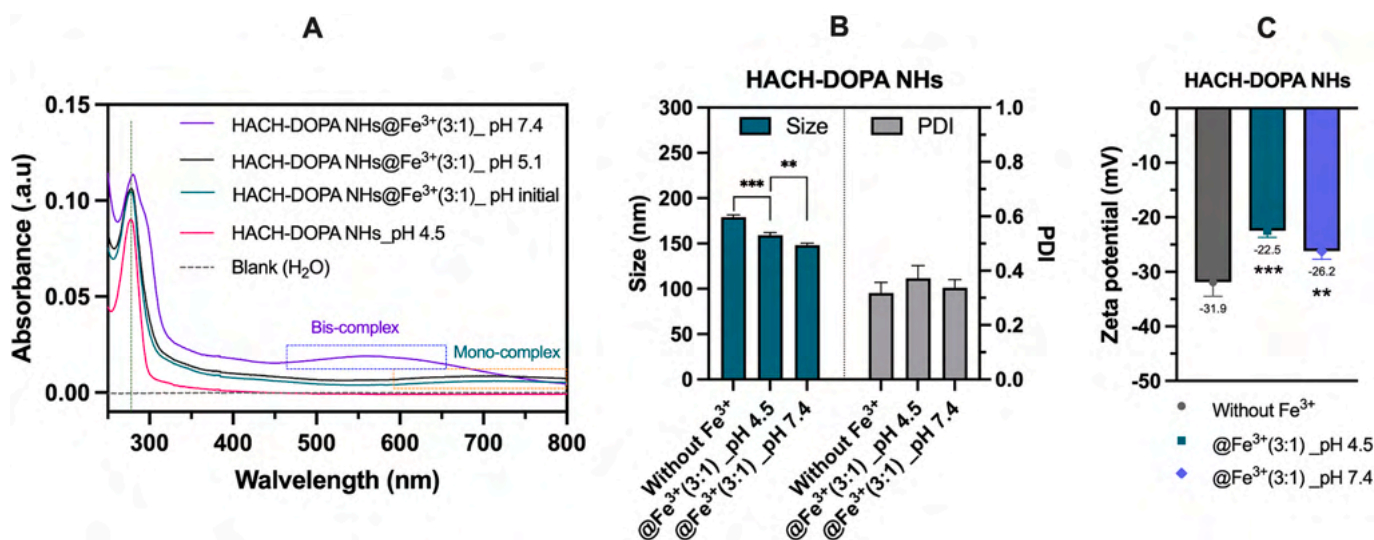

Fig. 7. (A) UV–visible spectra of HACH-DOPA nanogels and Fe^{3+} modified nanogel system (molar ratio of catechol: Fe^{3+} = 3:1) at acidic and physiological pH conditions. (B) Effect of pH and coordination bonds on the size, PDI, and (C) zeta potential of HACH-DOPA nanogels. * p < 0.05, ** p < 0.01, *** *p* < 0.001.
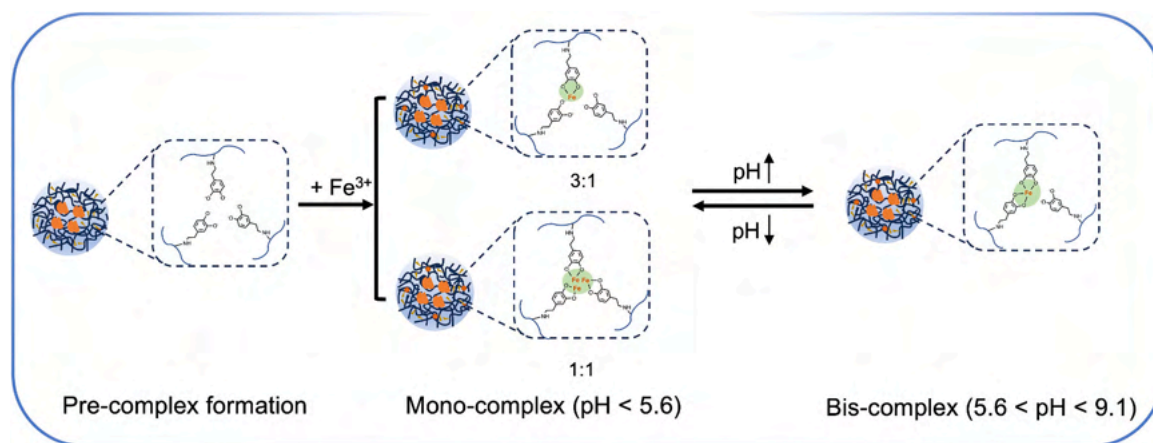
Fig. 8. Schematic of HACH-DOPA nanogels modification with ferric ion, and pH-dependent stoichiometry of Fe^{3+}-catechol complexes.
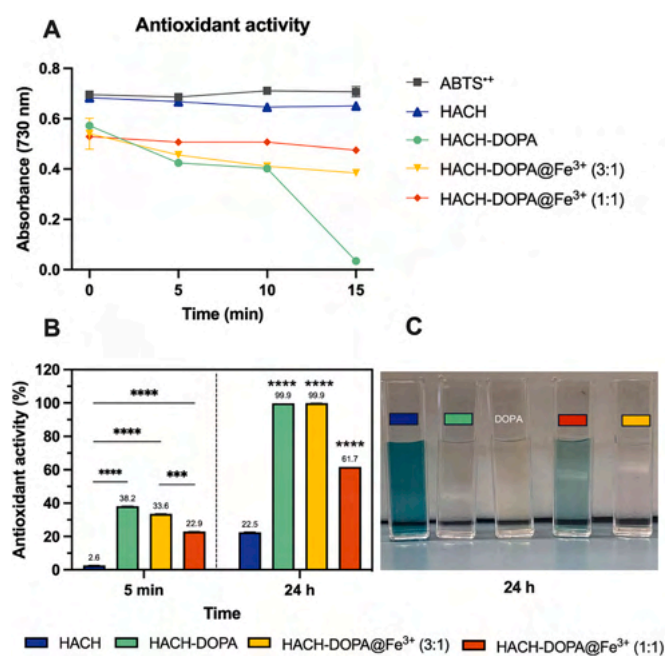

Fig. 9. Antioxidant activity evaluated by ABTS assay. (A) UV–Vis Abs ($\lambda = 730$ nm) trend as a function of time for different samples with a concentration of 1 mg/mL; (B) antioxidant activity (AA%) calculated after 5 min and 24 h of incubation. All the data are expressed as the mean value ± standard deviation. Results were obtained in triplicate (n = 3). * p < 0.05, ** p < 0.01, *** p < 0.001, **** p < 0.0001. (C) A representative photograph shows the colour change in the ABTS solution in the tube after incubation for 24 h.

were acquired using the Pin-Point mode, a fast-force volume modality of the Park microscope. The data were performed on several areas of each sample and repeated on three different preparations in order to ensure repeatability. Fig. 10 A shows the topographic images of the nanogels, highlighting the presence of several nanogel structures on the surface. A significant flattening of both HACH and HACH-DOPA nanogels in a liquid environment was observed, indicating the soft nature of these particles, while the iron-modified HACH-DOPA nanogels showed closer to a spherical structure. While the lateral dimension of the structures is difficult to measure in a liquid environment, we were able to determine with good accuracy the vertical size of the nanogels. Both the morphology images and the height analyses were performed using the free software Gwyddion. As shown in the right panels of Fig. 10A and C, the average height of HACH-DOPA@Fe^{3+} particles is significantly higher than the soft particles. The nanomechanical analyses of the very

same areas allowed us to measure the Young's modulus of the nanogels. The Young's modulus data were obtained using the free FCAnalysis software [55] to extract the nanomechanical properties from each force volume curve. Fig. 10B shows the histogram representing the differences in mechanical properties between the differently prepared nanogels. As expected, the modulation of nanogels with Fe^{3+} led to a significant increase in particle stiffness ($p < 0.01$). Notably, despite having similar vertical heights, the HACH-DOPA nanogels exhibited a significantly higher Young's modulus compared to the HACH nanogels. This difference could be attributed to the presence of more physical interactions during the formation of HACH-DOPA nanogels, resulting in tighter crosslinking.

3.7. Effect of nanogels on cell proliferation

The effect of HACH-DOPA and HACH-DOPA@Fe^{3+} nanogels on cell proliferation was evaluated over a wide concentration range of up to 72 h. In both cell lines, no significant decrease in cell proliferation was observed after 24 h and 48 h from the treatment with HACH-DOPA nanogels, compared to untreated cells (Fig. 11A, C), whereas after 72 h, a significant decrease in cell proliferation was observed only at the highest concentration tested (250 μg/mL, $p < 0.05$). Even Fe^{3+} modified HACH-DOPA nanogels determined significant cytotoxicity after 72 h of incubation at the highest concentration tested (250 μg/mL, Fig. 11B) in HUVEC, whereas in HDF HACH-DOPA@Fe^{3+} nanogels led to a significant decrease in cell proliferation already at 48 h (Fig. 11D). By considering these data, further cell experiments were carried out using the non-cytotoxic concentration of 100 μg/mL.

3.8. Evaluation of nanogel cellular uptake and distribution

To investigate the influence of dopamine or Fe^{3+}-modification on cellular internalisation, cell uptake studies of Rhod-labeled NHs were performed by flow cytometry on both HUVEC and HDF cells at a non-cytotoxic concentration (100 μg/mL) over time. As expected by using CD44 expressing cell lines, a time-dependent increase of the iMFI ratio, corresponding to the Rhod-labeled NHs internalisation, was observed after the incubation of all the nanogels in both HUVEC and HDF cells except for HACH-DOPA in HUVEC cells (Fig. 12A). However, the application of Fe^{3+} during both the synthesis and stiffness modification of Rhod-labeled nanogels led to the fluorescence quenching of Rhodamine B to some extent [56]. As a result, the Rhod-labeled HACH nanogels showed much higher fluorescence intensity compared to both Rhod-labeled HACH-DOPA and HACH-DOPA@Fe^{3+} nanogels at the same concentration (Fig. S6). Therefore, we normalised the data of iMFI ratio with consideration of the fluorescence quenching factor, as shown in panels b2-c2 of Fig. 12A. Interestingly, the normalised results of cellular
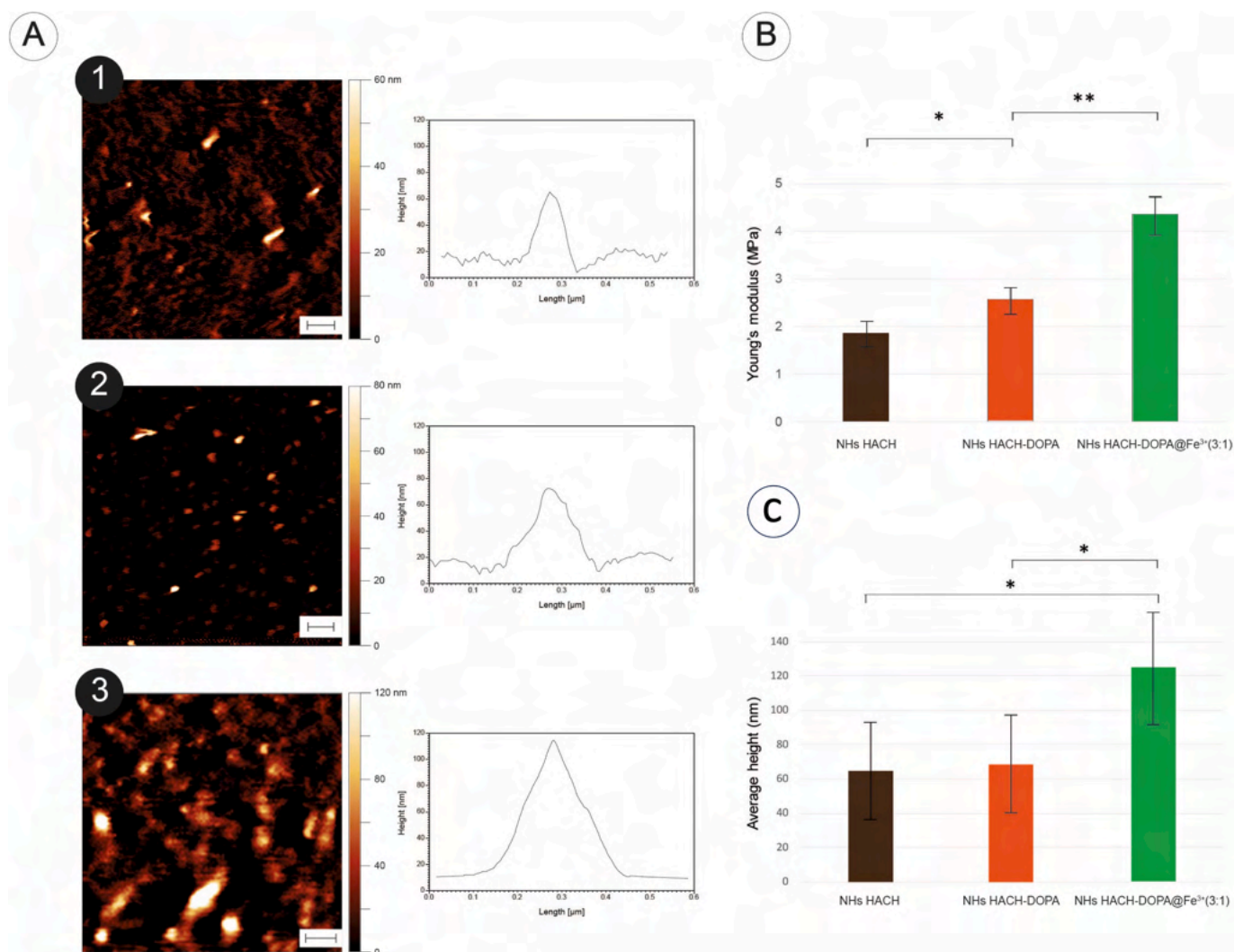
Fig. 10. (A) Typical images of hydrogel structures are imaged using AFM. Panel a refers to HACH particles, panel b to HACH-DOPA particles and panel c to the iron-modified HACH-DOPA nanogels. The right panels show some typical cross-sections on the identified structures. (B) Young's modulus of the differently prepared nanogels obtained from the Pin-Point AFM images. Results were obtained in triplicate (n = 3). * p < 0.05, ** p < 0.01. (C) Average vertical size (height) of the nanogels obtained through AFM images. The scale bar represents 500 nm. Results were obtained in triplicate (n = 3). * p < 0.05.

internalisation indicated that the modification of nanogels with both DOPA and Fe^{3+} enhanced cellular uptake. Specifically, compared with HACH-DOPA nanogels, the HACH-DOPA@Fe^{3+} nanogels showed approximately 5-fold and 3-fold enhanced internalisation after 24 h of incubation in HUVEC and HDF (Fig. 12A, panels b2-c2), respectively.

To support the previous data a qualitative investigation of the nanogels distribution into HUVEC and HDF was performed by confocal microscopy. Notably, the various nanogels accumulate into the HUVEC and HDF cytoplasm with a preferential accumulation into lysosomes, as shown in Fig. 12B and C. Overall, the enhanced cellular internalisation behaviour of the stiffness-increased nanogels (modified with iron ions) are similar to the findings from other studies [10,12,13]. This suggests their potential application in enhancing intracellular drug delivery efficiency.

4. Discussion

Inspired by tunable mechanical properties of mussel byssus, which are found in natural load-bearing materials primarily composed of organic macromolecules and inorganic metal ions, synthetic catechol or polyphenol-containing polymers have been widely explored for the preparation of biomaterials with remarkable mechanical properties and

improved adhesion behaviour by the formation of cooperative metal coordination sites with metal ion [57]. For instance, hyaluronic-based mussel-inspired polymers have been employed to develop bulk hydrogels [58–60] and biofilms [61,62] for tissue adhesive applications. However, combining the mechanical properties with the outstanding biological properties of hyaluronic acid derivative in the soft nanogel system remains a challenge in this relatively new field. Previous studies by our group have extensively investigated HACH-based nanogels, demonstrating their potential applications in drug delivery [23,35,36,63]. In this study, we present a strategy to combine multiple physical properties (*e.g.* nano size, self-assembly, injectable), biological properties (*e.g.* CD44 targeting, crossing bio-barriers), and tunable mechanical properties (soft and stiff) by employing coordination interaction between catechol and ferric ion. Our results highlight the importance of surface chemistry and stiffness of nanogels in their biological fates, such as their proper effect on *in vivo* circulation time and cellular internalisation, indicating potential application for enhancing effective drug delivery.

4.1. Synthesis and properties of HACH-DOPA polymer

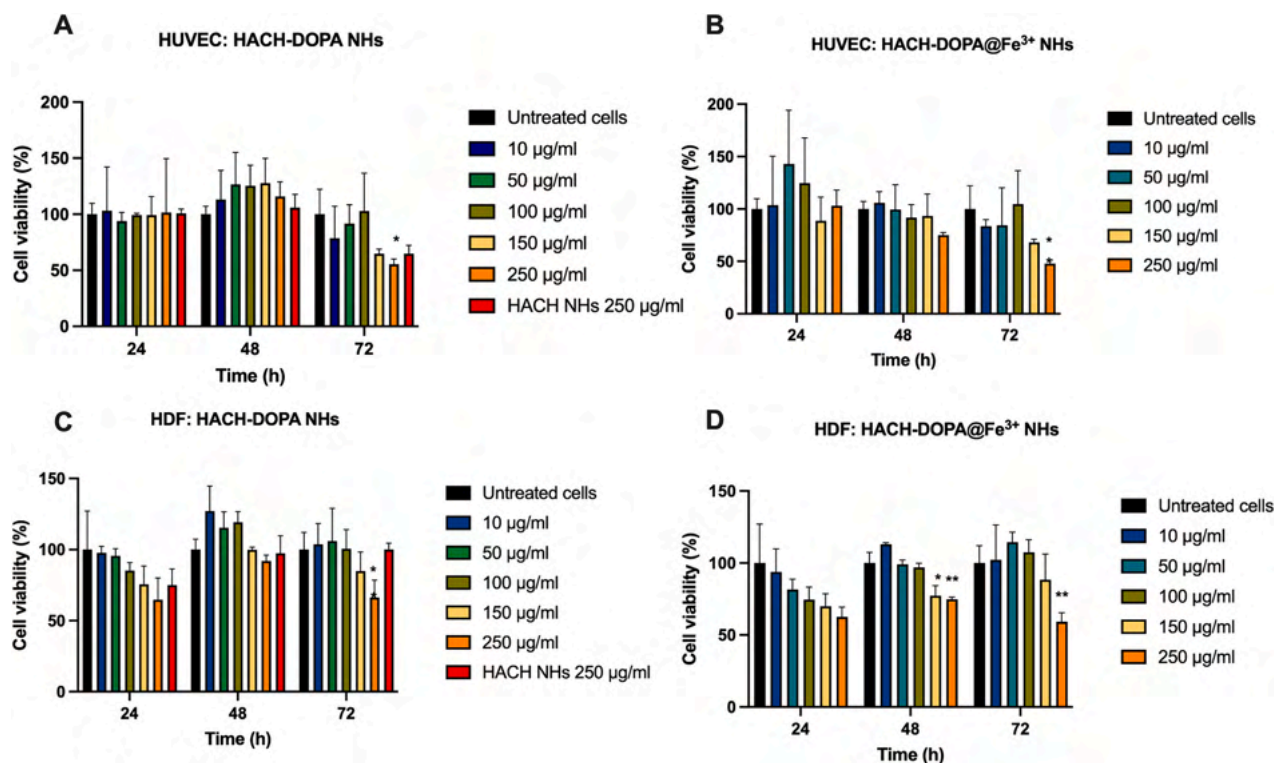The results provide evidence for the successful conjugation of HACH

Fig. 11. Effects of nanogels on HUVEC and HDF cell proliferation. Effects of HACH-DOPA nanogels (A, C) and Fe^{3+} modified HACH-DOPA nanogels (B, D) on HUVEC (A, B) and HDF (C, D) cells at increasing concentrations of polymer (10, 50, 100, 150 and 250 μg/mL). HACH nanogel (250 μg/mL) was used as the control. Cell viability was evaluated by WST-1 assay after incubation for 24, 48, and 72 h. Statistically significant difference *versus* untreated cells: * $p < 0.05$ and ** $p < 0.01$.

with DOPA, as confirmed by UV–vis absorption, ^{1}H NMR, FT-IR, and coordination reaction with Fe^{3+}. In the synthesis of DOPA-modified HACH, a molar ratio of -COOH: DOPA = 1:2 was selected for the reaction; however, the degree of substitution (DS%) was lower than that reported in other studies for DOPA-modified HA [33,60]. This is primarily due to two reasons, on the one hand, there was only no >90 % of -COOH available in HACH for further substitution, on the other hand, not all the carboxyl groups were exposed to the reaction due to the spontaneous formation of nanogels in amphipathic HACH. Similarly, not all the dopamine groups were exposed to the solvent during UV measurement, since nanogels, rather than a solution, would spontaneously form in water under the condition of sonication. Therefore, we speculate that the true content of dopamine in the polymer should be higher than what we measured by UV spectroscopy. As expected, the conjunction of DOPA onto HACH backbone endows the novel polymer with more interactions in aqueous environments for nanogel formation (Fig. 2). Indeed, the HACH-DOPA nanogels, whether in the presence of Fe^{3+} or not, exhibit smaller size and better stability when compared to those of HACH nanogels prepared under the same conditions, albeit with no significant difference (Figs. 3 and 6).

4.2. Stability and reversibility of HACH-DOPA@Fe^{3+} nanogels complex

As it is well known, the spontaneous autoxidation of dopamine occurs in basic aqueous media by dissolved oxygen. The initial autoxidation of dopamine leads to the formation of dopamine-semiquinone, which further oxidizes to dopamine-o-quinone. The subsequent step is the practically irreversible intramolecular cyclization to form dopachrome [64,65]. It has been confirmed that the intramolecular cyclization represents the rate-limiting step of oxidation reaction at pH values below 5 [65]. Interestingly, the dopamine moiety in HACH-DOPA remains stable within its mildly acidic nanogels, with a pH value of 4.5–4.8. Even in an aerobic environment, no obvious oxidation products were observed. This excellent stability could be attributed not only to

the slightly acidic nature of the system but also to the side-chain N-substitution of -NHCO- by the HACH macromolecule, in which the NH group in the dopamine derivative is not sufficiently nucleophilic to undergo cyclisation readily [66]. Moreover, M Salomäki M. et al. demonstrated that Fe (III) can enhance dopamine oxidation in acidic media under both aerobic and anaerobic conditions [65]. However, in the HACH-DOPA@Fe^{3+} nanogels system, no prominent oxidation products were detected by UV absorption when the pH was below 5.6. Instead, a mono-complex of catechol and Fe^{3+} is formed (Fig. 8A). The formation of complexes and dopamine oxidation strongly depends on pH value. As the pH increases from 5 to 7.4, the reversible mono-complex dominates transferred into bis-complex dominates. Simultaneously, oxidation products of dopamine semiquinone (with an absorption band at 305 nm) and dopamine-quinone (395 nm) were generated [65,67]. Notably, the oxidation reaction is reversible, and the UV absorption characteristics (indicated by the red dashed line in Fig. S3) recover when the pH recovers from 7.4 to 5.0. Although the tris-complex would form at pH values above 9.1 [31], our focus is mainly limited to the pH range from slightly acidic conditions to physiological conditions, considering the application of injectable soft nanogels. Furthermore, we also investigated the effect of both different ratios of Fe^{3+} and pH values (ranging from initial to 12) on the nanogel systems. The results indicated that the HACH-DOPA@Fe^{3+} complexes at a ratio of 3:1 exhibited good reversibility within pH values ranging from approximately 4 to 11. However, at a higher Fe^{3+} ratio of 1:1, more irreversible oxidation products were generated when the nanogels were exposed to strong alkaline conditions (Fig. S4). Consequently, the UV absorption was unable to recover to its initial state.

4.3. Influence of dopamine and Fe^{3+} on cytocompatibility

Considering both the effective modification as well as stability of nanogels and the possible cytotoxicity induced by high concentrations of metal ions, we selected the ratio of 3:1 between catechol and Fe^{3+} as the
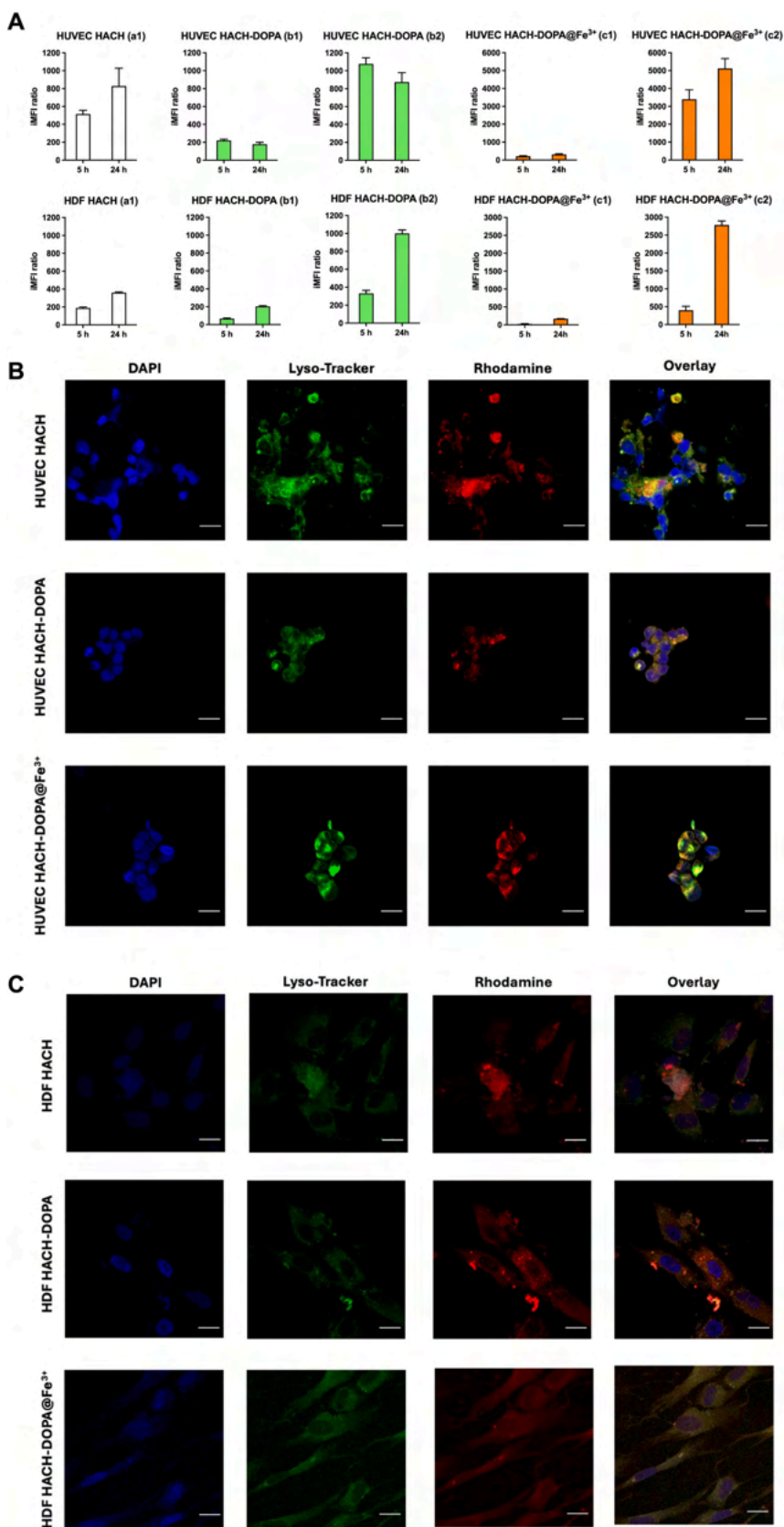
(caption on next page)

Fig. 12. Cellular uptake and distribution of nanogels. A) The graphs represent the cytofluorimetric evaluation of the cellular uptake of fluorescently labeled NHs (HACH, HACH-DOPA, and HACH-DOPA@Fe^{3+}) in HUVEC and HDF cells at 5 and 24 h of incubation. The data are presented as original data (a1, b1, c1) and normalised data according to fluorescence intensity (b2, c2), respectively. Fluorescent signals were detected using a flow cytometer to measure the intracellular amount of Rhod-labeled NHs that was expressed as iMFI ratio *versus* untreated cells. B) HUVEC and C) HDF representative images of the intracellular localisation of the fluorescently labeled nanogels at 24 h of incubation. Confocal images show cell nuclei stained with DAPI (blue), Lyso-Tracker Green (green), Rhodamine (red) and overlay (magnification 40× and scale bar 20 μm).

test samples for the modulation of the formulation. Previous studies have demonstrated that dopamine and its derivatives can induce adult neural precursor cell proliferation [68], enhance endothelial cell affinity, promote cellular proliferation [69,70]. Notably, HACH-DOPA nanogels do not affect cell proliferation of both HUVEC and HDF cell lines up to 150 μg/mL (Fig. 11A and D). The present study suggests HACH-DOPA@Fe^{3+} nanogels as promising tools for biomedical applications, although their cytocompatibility is slightly affected by Fe^{3+} concentrations being the highest not-cytotoxic concentration (100 μg/mL) lower than that of HACH-DOPA nanogels (150 μg/mL) in HDF (Fig. 11). The concentration of Fe^{3+} in the nanogels@Fe^{3+} complex is approximately 60 μM, which is unlikely to induce significant cytotoxicity. It has been demonstrated that polymer-carriers containing a higher concentration of Fe^{3+} have promising applications in cell transplantation and drug delivery [71,72].

4.4. The possible influence of mechanical properties on biological behaviour

In recent decades, nanomedicine has been developed to promote drug delivery efficiency by enhancing the permeability and retention (EPR) effect [73]. However, one of the major challenges in drug delivery is the quick clearance of nanoparticles from blood circulation by macrophages in the reticuloendothelial system (RES) after *i.v.* injection, which limits the delivery of drugs to the targeted site [74]. Therefore, effective strategies for decreasing blood clearance, increasing targeted accumulation and promoting cellular internalisation are highly desirable. The mechanical properties of nanomedicine have been demonstrated to play a crucial role in blood circulation time and cellular internalisation [75]. Zheng Li et al. proposed a strategy of mechanoboosting nanomedicine by taking full advantage of nanogels mechanical properties to overcome pathophysiological barriers in RES-blockade and drug delivery [13]. Specifically, stiff nanogels with poor deformability can enhance cellular uptake and prolong blood circulation by RES-blockade. On the other hand, soft nanogels can achieve efficient tumour penetration and accumulation. The stiffness-dependent RES-blockade strategy demonstrated improved effective drug delivery, benefitting from the combined advantages of nanogels with distinctive stiffness at different drug delivery stages [13]. In this work, surface chemistry modification of nanogels, including surface hydrophobicity and surface charge, combined with the internal crosslinking strength, made HACH-DOPA@Fe^{3+} nanogels display significantly increased stiffness (Fig. 10B), resulting in enhanced cellular internalisation behaviour (Fig. 12A). Compared to HACH nanogels, HACH-DOPA nanogels also exhibited enhanced cellular uptake, likely attributed to the altered surface hydrophobicity of nanoparticles. Additionally, incomplete removal of iron ions coordinated with catechol groups may have occurred during the purification process of Rhod-labeled HACH-DOPA, leading to an increase in the stiffness of the nanogels, to some extent, and subsequently promoting cellular internalisation.

Clinical application is the final target of nanomedicines and nanotherapeutic strategy. Due to the injectable and CD44 targeting characteristics, these tunable HACH-DOPA nanogels are promising to enhance intracellular drug delivery in the treatment of diseases where CD44 overexpression occurs by *i.v.* or topical *in-situ* administration. This work has several critical significances. First, dopamine-modified amphipathic HACH polymer that endows various properties was obtained, including better self-assembly capability, drug loading efficiency, stability,

antioxidant activity, and modified surface hydrophobicity. On the other hand, we provide valuable insights into the modulation of nanogel mechanical properties by introducing metal coordination interactions. However, several aspects require further exploration. We investigated the cell uptake behaviour of modified nanogels, but how the surface and stiffness modification affect their *in vivo* distribution and blood circulation time remains unclear. Furthermore, assessment of the drug loading efficiency for other therapeutic agents (*e.g.*, antitumor molecules, hydrophilic antibiotics, *etc.*) and further *in vivo* evaluation of the therapeutic efficiency of the nanogels are still necessary.

5. Conclusions

In summary, this work proposes valuable insights into the *stiffness* modulation of soft nanogel by bio-inspired strategy, intending to develop a new carrier for potential applications in drug delivery. The HACH polymer was successfully modified by grafting dopamine onto the HA backbone, obtaining a novel amphipathic polymer capable of self-assembly into nanogels in an aqueous environment. These nanogels exhibited excellent properties, including antioxidant activity and efficient encapsulation ability of hydrophobic drugs. The introduction of catechol groups allowed for the modulation of nanogel stiffness *via* coordination interaction with Fe^{3+}, with a molar ratio of 3:1 between catechol groups and Fe^{3+} for the modification. Besides, it was demonstrated that nanogels@Fe^{3+} mono-complexes dominate formed at slightly acidic conditions, which transitioned into bis-complexes as the pH increased to physiological conditions. Moreover, cell proliferation assays indicated no obvious cytotoxicity, and it was observed that the modified nanogels displayed enhanced cellular internalisations. The present modulation strategy, inspired by metal-catechol coordination interaction in mussel nature, holds great potential for expanding the applications of HACH nanogels in enhancing intracellular drug delivery.

CRediT authorship contribution statement

Ju Wang: Writing – review & editing, Writing – original draft, Validation, Methodology, Investigation, Formal analysis, Data curation, Conceptualization. **Benedetta Brugnoli:** Writing – review & editing, Methodology, Investigation, Data curation. **Federica Foglietta:** Writing – review & editing, Validation, Methodology, Investigation, Data curation. **Ilaria Andreana:** Writing – review & editing, Validation, Methodology, Investigation, Data curation. **Giovanni Longo:** Writing – review & editing, Methodology, Investigation, Data curation. **Simone Dinarelli:** Writing – review & editing, Methodology, Investigation, Data curation. **Marco Girasole:** Writing – review & editing, Supervision. **Loredana Serpe:** Writing – review & editing, Supervision. **Silvia Arpicco:** Writing – review & editing, Supervision, Resources. **Iolanda Francolini:** Writing – review & editing, Supervision. **Chiara Di Meo:** Writing – review & editing, Supervision, Project administration. **Pietro Matricardi:** Writing – review & editing, Writing – original draft, Supervision, Project administration, Funding acquisition, Conceptualization.

Declaration of competing interest

The authors have no conflicts of interest to declare.

Data availability

Data will be made available on request.

Appendix A. Supplementary data

Supplementary data to this article can be found online at https://doi.org/10.1016/j.ijbiomac.2024.135553.

References

[1] B.D. Chithrani, A.A. Ghazani, W.C. Chan, Determining the size and shape dependence of gold nanoparticle uptake into mammalian cells, Nano Lett. 6 (4) (2006) 662–668.

[2] N. Hoshyar, S. Gray, H. Han, G. Bao, The effect of nanoparticle size on in vivo pharmacokinetics and cellular interaction, Nanomedicine 11 (6) (2016) 673–692.

[3] A. Albanese, P.S. Tang, W.C. Chan, The effect of nanoparticle size, shape, and surface chemistry on biological systems, Annu. Rev. Biomed. Eng. 14 (2012) 1–16.

[4] X. Duan, Y. Li, Physicochemical characteristics of nanoparticles affect circulation, biodistribution, cellular internalization, and trafficking, Small 9 (9–10) (2013) 1521–1532.

[5] R.E. Mebius, G. Kraal, Structure and function of the spleen, Nat. Rev. Immunol. 5 (8) (2005) 606–616.

[6] N. Kol, Y. Shi, M. Tsvitov, D. Barlam, R.Z. Shneck, M.S. Kay, I. Rousso, A stiffness switch in human immunodeficiency virus, Biophys. J. 92 (5) (2007) 1777–1783.

[7] P.-H. Wu, D.R.-B. Aroush, A. Asnacios, W.-C. Chen, M.E. Dokukin, B.L. Doss, P. Durand-Smet, A. Ekpenyong, J. Guck, N.V. Guz, A comparison of methods to assess cell mechanical properties, Nat. Methods 15 (2018) 491–498.

[8] Z. Li, C. Xiao, T. Yong, Z. Li, L. Gan, X. Yang, Influence of nanomedicine mechanical properties on tumor targeting delivery, Chem. Soc. Rev. 49 (8) (2020) 2273–2290.

[9] Y. Hui, X. Yi, F. Hou, D. Wibowo, F. Zhang, D. Zhao, H. Gao, C.-X. Zhao, Role of nanoparticle mechanical properties in cancer drug delivery, ACS Nano 13 (7) (2019) 7410–7424.

[10] A.C. Anselmo, M. Zhang, S. Kumar, D.R. Vogus, S. Menegatti, M.E. Helgeson, S. Mitragotri, Elasticity of nanoparticles influences their blood circulation, phagocytosis, and endocytosis, and targeting, ACS Nano 9 (3) (2015) 3169–3177.

[11] H. Chen, Z. Gu, H. An, C. Chen, J. Chen, R. Cui, S. Chen, W. Chen, X. Chen, X. Chen, Z. Chen, B. Ding, Q. Dong, Q. Fan, T. Fu, D. Hou, Q. Jiang, H. Ke, X. Jiang, G. Liu, S. Li, T. Li, Z. Liu, G. Nie, M. Ovais, D. Pang, N. Qiu, Y. Shen, H. Tian, C. Wang, H. Wang, Z. Wang, H. Xu, J.-F. Xu, X. Yang, S. Zhu, X. Zheng, X. Zhang, Y. Zhao, W. Tan, X. Zhang, Y. Zhao, Precise nanomedicine for intelligent therapy of cancer, SCIENCE CHINA Chem. 61 (12) (2018) 1503–1552.

[12] J. Sun, L. Zhang, J. Wang, Q. Feng, D. Liu, Q. Yin, D. Xu, Y. Wei, B. Ding, X. Shi, Tunable rigidity of (polymeric core)–(lipid shell) nanoparticles for regulated cellular uptake, Adv. Mater. 27 (8) (2015) 1402–1407.

[13] Z. Li, Y. Zhu, H. Zeng, C. Wang, C. Xu, Q. Wang, H. Wang, S. Li, J. Chen, C. Xiao, X. Yang, Z. Li, Mechano-boosting nanomedicine antitumour efficacy by blocking the reticuloendothelial system with stiff nanogels, Nat. Commun. 14 (1) (2023) 1437.

[14] Y. Chen, S. De Koker, B.G. De Geest, Engineering strategies for lymph node targeted immune activation, Acc. Chem. Res. 53 (10) (2020) 2055–2067.

[15] D. Christensen, M. Henriksen-Lacey, A.T. Kamath, T. Lindenstrøm, K.S. Korsholm, J.P. Christensen, A.-F. Rochat, P.-H. Lambert, P. Andersen, C.-A. Siegrist, Y. Perrie, E.M. Agger, A cationic vaccine adjuvant based on a saturated quaternary ammonium lipid have different in vivo distribution kinetics and display a distinct CD4 T cell-inducing capacity compared to its unsaturated analog, J. Control. Release 160 (3) (2012) 468–476.

[16] N. Zoratto, E. Montanari, M. Viola, J. Wang, T. Coviello, C. Di Meo, P. Matricardi, Strategies to load therapeutics into polysaccharide-based nanogels with a focus on microfluidics: a review, Carbohydr. Polym. 266 (2021) 118119.

[17] J. Wang, M. Viola, C. Migliorini, L. Paoletti, S. Arpicco, C. Di Meo, P. Matricardi, Polysaccharide-based Nanogels to overcome mucus, skin, cornea, and blood-brain barriers: a review, Pharmaceutics 15 (10) (2023) 2508.

[18] K. Hemmati, M. Ghaemy, Synthesis of new thermo/pH sensitive drug delivery systems based on tragacanth gum polysaccharide, Int. J. Biol. Macromol. 87 (2016) 415–425.

[19] K. Hemmati, A. Masoumi, M. Ghaemy, Synthesis and characterization of pH-responsive nanohydrogels as biocompatible drug carriers based on chemically modified tragacanth gum polysaccharide, RSC Adv. 5 (104) (2015) 85310–85318.

[20] R.C. Gupta, R. Lall, A. Srivastava, A. Sinha, Hyaluronic acid: molecular mechanisms and therapeutic trajectory, Frontiers in Veterinary Science 6 (2019) 192.

[21] M. Ashrafizadeh, S. Mirzaei, M.H. Gholami, F. Hashemi, A. Zabolian, M. Raei, K. Hushmandi, A. Zarrabi, N.H. Voelcker, A.R. Aref, M.R. Hamblin, R.S. Varma, S. Samarghandian, I.J. Arostegi, M. Alzola, A.P. Kumar, V.K. Thakur, N. Nabavi, P. Makvandi, F.R. Tay, G. Orive, Hyaluronic acid-based nanoplatforms for doxorubicin: a review of stimuli-responsive carriers, co-delivery and resistance suppression, Carbohydr. Polym. 272 (2021) 118491.

[22] A.V. Kabanov, S.V. Vinogradov, Nanogels as pharmaceutical carriers: finite networks of infinite capabilities, Angew. Chem. Int. Ed. 48 (30) (2009) 5418–5429.

[23] E. Montanari, P. Mancini, F. Galli, M. Varani, I. Santino, T. Coviello, L. Mosca, P. Matricardi, F. Rancan, C. Di Meo, Biodistribution and intracellular localization of hyaluronan and its nanogels. A strategy to target intracellular S. Aureus in persistent skin infections, J. Control. Release 326 (2020) 1–12.

[24] M. Li, Z. Gao, J. Cui, Modulation of Colloidal Particle Stiffness for the Exploration of Bio–Nano Interactions, Langmuir 38 (22) (2022) 6780–6785.

[25] W. Zhang, R. Wang, Z. Sun, X. Zhu, Q. Zhao, T. Zhang, A. Cholewinski, F.K. Yang, B. Zhao, R. Pinnaratip, Catechol-functionalized hydrogels: biomimetic design, adhesion mechanism, and biomedical applications, Chem. Soc. Rev. 49 (2) (2020) 433–464.

[26] A. Andersen, M. Krogsgaard, H. Birkedal, Mussel-inspired self-healing double-cross-linked hydrogels by controlled combination of metal coordination and covalent cross-linking, Biomacromolecules 19 (5) (2017) 1402–1409.

[27] R. Ganguly, P. Saha, S.L. Banerjee, A. Pich, N.K. Singha, Stimuli-responsive block copolymer micelles based on mussel-inspired metal-coordinated supramolecular networks, Macromol. Rapid Commun. 42 (17) (2021) 2100312.

[28] G. Janarthanan, I. Noh, Recent trends in metal ion based hydrogel biomaterials for tissue engineering and other biomedical applications, Journal of Materials Science & Technology 63 (2021) 35–53.

[29] N. Holten-Andersen, M.J. Harrington, H. Birkedal, B.P. Lee, P.B. Messersmith, K.Y.C. Lee, J.H. Waite, pH-induced metal-ligand cross-links inspired by mussel yield self-healing polymer networks with near-covalent elastic moduli, Proc. Natl. Acad. Sci. 108 (7) (2011) 2651–2655.

[30] F. Shuai, Y. Zhang, Y. Yin, H. Zhao, X. Han, Fabrication of an injectable iron (III) crosslinked alginate-hyaluronic acid hydrogel with shear-thinning and antimicrobial activities, Carbohydr. Polym. 260 (2021) 117777.

[31] J. Ryu, S. Kim, I. Oh, S. Kato, T. Kosuge, A.V. Sokolova, J. Lee, H. Otsuka, D. Sohn, Internal structure of hyaluronic acid hydrogels controlled by iron (III) ion–catechol complexation, Macromolecules 52 (17) (2019) 6502–6513.

[32] J. Xiong, Z.R. Yang, N. Lv, K. Du, H. Suo, S. Du, J. Tao, H. Jiang, J. Zhu, Self-adhesive hyaluronic acid/antimicrobial peptide composite hydrogel with antioxidant capability and photothermal activity for infected wound healing, Macromol. Rapid Commun. 43 (18) (2022) 2200176.

[33] J. Lee, K. Chang, S. Kim, V. Gite, H. Chung, D. Sohn, Phase controllable hyaluronic acid hydrogel with iron (III) ion–catechol induced dual cross-linking by utilizing the gap of gelation kinetics, Macromolecules 49 (19) (2016) 7450–7459.

[34] J.M. Rios de la Rosa, P. Pingrajai, M. Pelliccia, A. Spadea, E. Lallana, A. Gennari, I.J. Stratford, W. Rocchia, A. Tirella, N. Tirelli, Binding and internalization in receptor-targeted carriers: the complex role of CD44 in the uptake of hyaluronic acid-based nanoparticles (siRNA delivery), Adv. Healthc. Mater. 8 (24) (2019) 1901182.

[35] E. Montanari, C. Di Meo, S. Sennato, A. Francioso, A.L. Marinelli, F. Ranzo, S. Schippa, T. Coviello, F. Bordi, P. Matricardi, Hyaluronan-cholesterol nanohydrogels: characterisation and effectiveness in carrying alginate lyase, N. Biotechnol. 37 (2017) 80–89.

[36] N. Zoratto, L. Forcina, R. Matassa, L. Mosca, G. Familiari, A. Musarò, M. Mattei, T. Coviello, C. Di Meo, P. Matricardi, Hyaluronan-cholesterol nanogels for the enhancement of the ocular delivery of therapeutics, Pharmaceutics 13 (11) (2021) 1781.

[37] M. Viola, C. Migliorini, P. Matricardi, C. Di Meo, Synthesis and characterization of a novel amphiphilic polyacrylate-cholesterol derivative as promising material for pharmaceutical and cosmetic applications, Eur. Polym. J. 184 (2023) 111774.

[38] F. Scognamiglio, A. Travan, M. Borgogna, I. Donati, E. Marsich, J.W.A.M. Bosmans, L. Perge, M.P. Foulc, N.D. Bouvy, S. Paoletti, Enhanced bioadhesivity of dopamine-functionalized polysaccharidic membranes for general surgery applications, Acta Biomater. 44 (2016) 232–242.

[39] M. Yang, S.Y. Lee, S. Kim, J.S. Koo, J.-H. Seo, D.I. Jeong, C. Hwang, J. Lee, H.-J. Cho, Selenium and dopamine-crosslinked hyaluronic acid hydrogel for chemophotothermal cancer therapy, J. Control. Release 324 (2020) 750–764.

[40] M. Müller, B. Keßler, Deposition from dopamine solutions at Ge substrates: an in situ ATR-FTIR study, Langmuir 27 (20) (2011) 12499–12505.

[41] E. Montanari, S. Capece, C. Di Meo, M. Meringolo, T. Coviello, E. Agostinelli, P. Matricardi, Hyaluronic acid nanohydrogels as a useful tool for BSAO immobilization in the treatment of melanoma cancer cells, Macromol. Biosci. 13 (9) (2013) 1185–1194.

[42] K. Kadota, M. Tanaka, H. Nishiyama, J.Y. Tse, H. Uchiyama, Y. Shirakawa, Y. Tozuka, An effective approach to modify the inhalable betamethasone powders based on morphology and surface control using a biosurfactant, Powder Technol. 376 (2020) 517–526.

[43] H. Lee, N.F. Scherer, P.B. Messersmith, Single-molecule mechanics of mussel adhesion, Proc. Natl. Acad. Sci. 103 (35) (2006) 12999–13003.

[44] J. Yu, W. Wei, E. Danner, R.K. Ashley, J.N. Israelachvili, J.H. Waite, Mussel protein adhesion depends on interprotein thiol-mediated redox modulation, Nat. Chem. Biol. 7 (9) (2011) 588–590.

[45] H. Zhao, J.H. Waite, Linking adhesive and structural proteins in the attachment plaque of Mytilus californianus, J. Biol. Chem. 281 (36) (2006) 26150–26158.

[46] W. Sun, B. Xue, Q. Fan, R. Tao, C. Wang, X. Wang, Y. Li, M. Qin, W. Wang, B. Chen, Molecular engineering of metal coordination interactions for strong, tough, and fast-recovery hydrogels, science, Advances 6 (16) (2020) eaaz9531.

[47] M.S. Menyo, C.J. Hawker, J.H. Waite, Versatile tuning of supramolecular hydrogels through metal complexation of oxidation-resistant catechol-inspired ligands, Soft Matter 9 (43) (2013) 10314–10323.

[48] S. Li, L. Wang, X. Yu, C. Wang, Z. Wang, Synthesis and characterization of a novel double cross-linked hydrogel based on Diels-Alder click reaction and coordination bonding, Mater. Sci. Eng. C 82 (2018) 299–309.

[49] C.-F. Su, Y.-F. Chen, Y.-J. Tsai, S.-M. Weng, J.-S. Jan, Antioxidant activity of linear and star-shaped polypeptides modified with dopamine and glutathione, Eur. Polym. J. 152 (2021) 110497.

[50] K. Kanazawa, H. Sakakibara, High content of dopamine, a strong antioxidant, in cavendish banana, J. Agric. Food Chem. 48 (3) (2000) 844–848.

[51] F. Xia, K. Youcef-Toumi, Review: advanced atomic force microscopy modes for biomedical research, Biosensors 12 (12) (2022) 1116.

[52] Y.F. Dufrêne, A. Viljoen, J. Mignolet, M. Mathelié-Guinlet, AFM in cellular and molecular microbiology, Cell. Microbiol. 23 (7) (2021) e13324.

[53] S. Dinarelli, G. Longo, S. Krumova, S. Todinova, A. Danailova, S. Taneva, E. Lenzi, V. Mussi, M. Girasole, Insights into the morphological pattern of erythrocytes' aging: coupling quantitative AFM data to microcalorimetry and Raman spectroscopy, J. Mol. Recognit. 31 (11) (2018) e2732.

[54] E. Lenzi, S. Dinarelli, G. Longo, M. Girasole, V. Mussi, Multivariate analysis of mean Raman spectra of erythrocytes for a fast analysis of the biochemical signature of ageing, Talanta 221 (2021) 121442.

[55] S. Dinarelli, M. Girasole, G. Longo, FC_analysis: a tool for investigating atomic force microscopy maps of force curves, BMC Bioinformatics 19 (2018) 1–12.

[56] Z. Liu, N. Li, P. Liu, Z. Qin, T. Jiao, Highly sensitive detection of iron ions in aqueous solutions using fluorescent chitosan nanoparticles functionalized by rhodamine B, ACS Omega 7 (6) (2022) 5570–5577.

[57] Y. Mu, Q. Sun, B. Li, X. Wan, Advances in the synthesis and applications of mussel-inspired polymers, Polym. Rev. 63 (1) (2023) 1–39.

[58] J. Shin, J.S. Lee, C. Lee, H.J. Park, K. Yang, Y. Jin, J.H. Ryu, K.S. Hong, S.H. Moon, H.M. Chung, Tissue adhesive catechol-modified hyaluronic acid hydrogel for effective, minimally invasive cell therapy, Adv. Funct. Mater. 25 (25) (2015) 3814–3824.

[59] Y. Yuan, S. Shen, D. Fan, A physicochemical double cross-linked multifunctional hydrogel for dynamic burn wound healing: shape adaptability, injectable self-healing property and enhanced adhesion, Biomaterials 276 (2021) 120838.

[60] Y. Zhou, L. Kang, Z. Yue, X. Liu, G.G. Wallace, Composite tissue adhesive containing catechol-modified hyaluronic acid and poly-l-lysine, ACS Appl. Bio Mater. 3 (1) (2019) 628–638.

[61] A.I. Neto, A.C. Cibrão, C.R. Correia, R.R. Carvalho, G.M. Luz, G.G. Ferrer, G. Botelho, C. Picart, N.M. Alves, J.F. Mano, Nanostructured polymeric coatings based on chitosan and dopamine-modified hyaluronic acid for biomedical applications, Small 10 (12) (2014) 2459–2469.

[62] A.I. Neto, N.L. Vasconcelos, S.M. Oliveira, D. Ruiz-Molina, J.F. Mano, High-throughput topographic, mechanical, and biological screening of multilayer films containing mussel-inspired biopolymers, Adv. Funct. Mater. 26 (16) (2016) 2745–2755.

[63] E. Montanari, C. Di Meo, T. Coviello, V. Gueguen, G. Pavon-Djavid, P. Matricardi, Intracellular delivery of natural antioxidants via hyaluronan nanohydrogels, Pharmaceutics 11 (10) (2019) 532.

[64] N. Umek, B. Geršak, N. Vintar, M. Šoštarič, J. Mavri, Dopamine autoxidation is controlled by acidic pH, Front. Mol. Neurosci. 11 (2018) 467.

[65] M. Salomäki, L. Marttila, H. Kivelä, T. Ouvinen, J. Lukkari, Effects of pH and oxidants on the first steps of polydopamine formation: a thermodynamic approach, J. Phys. Chem. B 122 (24) (2018) 6314–6327.

[66] J. Borovansky, R. Edge, E.J. Land, S. Navaratnam, S. Pavel, C.A. Ramsden, P. A. Riley, N.P. Smit, Mechanistic studies of melanogenesis: the influence of N-substitution on dopamine quinone cyclization, Pigment Cell Res. 19 (2) (2006) 170–178.

[67] M. Bisaglia, S. Mammi, L. Bubacco, Kinetic and structural analysis of the early oxidation products of dopamine: analysis of the interactions with α-synuclein, J. Biol. Chem. 282 (21) (2007) 15597–15605.

[68] G.C. O'Keeffe, P. Tyers, D. Aarsland, J.W. Dalley, R.A. Barker, M.A. Caldwell, Dopamine-induced proliferation of adult neural precursor cells in the mammalian subventricular zone is mediated through EGF, Proc. Natl. Acad. Sci. 106 (21) (2009) 8754–8759.

[69] H.-Y. Mi, X. Jing, J.A. Thomsom, L.-S. Turng, Promoting endothelial cell affinity and antithrombogenicity of polytetrafluoroethylene (PTFE) by mussel-inspired modification and RGD/heparin grafting, J. Mater. Chem. B 6 (21) (2018) 3475–3485.

[70] T.-D. Zhang, X. Deng, Y.-F. Wang, X.-T. Wang, X. Zhang, L.-L. Chen, X. Cao, Y.-Z. Zhang, C.-Y. Zhang, X. Zheng, Layer-by-layer coating of polyvinylamine and dopamine-modified hyaluronic acid inhibits the growth of bacteria and tumor cell lines on the surface of materials, Appl. Surf. Sci. 530 (2020) 147197.

[71] M. Anamizu, Y. Tabata, Design of injectable hydrogels of gelatin and alginate with ferric ions for cell transplantation, Acta Biomater. 100 (2019) 184–190.

[72] Y. Huang, Z. Tang, S. Peng, J. Zhang, W. Wang, Q. Wang, W. Lin, X. Lin, X. Zu, H. Luo, G. Yi, pH/redox/UV irradiation multi-stimuli responsive nanogels from star copolymer micelles and Fe3+ complexation for "on-demand" anticancer drug delivery, React. Funct. Polym. 149 (2020) 104532.

[73] J. Shi, P.W. Kantoff, R. Wooster, O.C. Farokhzad, Cancer nanomedicine: progress, challenges and opportunities, Nat. Rev. Cancer 17 (1) (2017) 20–37.

[74] S.A. MacParland, K.M. Tsoi, B. Ouyang, X.Z. Ma, J. Manuel, A. Fawaz, M. A. Ostrowski, B.A. Alman, A. Zilman, W.C. Chan, I.D. McGilvray, Phenotype determines nanoparticle uptake by human macrophages from liver and blood, ACS Nano 11 (3) (2017) 2428–2443.

[75] Z. Li, C. Xiao, T. Yong, Z. Li, L. Gan, X. Yang, Influence of nanomedicine mechanical properties on tumor targeting delivery, Chem. Soc. Rev. 49 (8) (2020) 2273–2290.